5-2014

Effects of Froude Scaling on Velocity-Induced Vortices in Physical Models

Michael S. Budge
Utah State University

EFFECTS OF FROUDE SCALING ON VELOCITY-INDUCED VORTICES IN PHYSICAL MODELS

By

Michael S. Budge

A thesis submitted in partial fulfillment
of the requirements for the degree

of

MASTER OF SCIENCE

in

Civil and Environmental Engineering

Approved:

_____	_____
Steven Barfuss Major Professor	William Rahmeyer Committee Member
_____	_____
Paul Barr Committee Member	Steven Beck Assistant Dean School of Graduate Studies

UTAH STATE UNIVERSITY
Logan, Utah

2014

ABSTRACT

Effects of Froude Scaling on Velocity-Induced Vortices in Physical Models

by

Michael S. Budge, Master of Science

Utah State University, 2014

Major Professor: Steven L. Barfuss
Department: Civil and Environmental Engineering

Velocity-induced vortices are common occurrences at hydraulic intakes and are detrimental to the operation and efficiency of hydraulic structures. Velocity-induced vortices also form in physical hydraulic models and although Froude scaling principles account for initial and gravity forces, the scale effects associated with vortices in Froude are less certain. This work examines scale effects on vortex formation in physical models through the use of four identical experiments built at differing Froude scales with the largest of the four being defined as a prototype. Each experiment created velocity-induced vortices at the intake to a sluice gate. The unique approach conditions caused surface swirl, downward velocity towards the sluice gate opening, and vortex flow. This study contributes to the existing literature by providing a set of both qualitative and quantitative observations made from images in multiple perspectives and measured data.

It was found that vortex behavior scaled as expected using Froude scaling principles with relatively small length ratios (~1:2 to ~1:3). As model size decreased, scaling accuracy decreased due to low approach and vortex tangential velocities. For

example, identical conditions in an experimental model at a scale 8 times smaller than the prototype experienced vortex formation of vastly decreased strength and size. Instead of an air core vortex, only a weak vortex having a shallow surface depression and swirl was formed at the same flow condition. Other model sizes showed a clear trend of decreasing vortex size and strength as the model size decreased. Decrease in strength is due largely to a decrease of approach and tangential velocity in the smaller models. Results from this study are also presented visually as a series of photographs and overlaid outline profiles for comparison. Additionally, other quantifiable results including dimensionless parameters are reported.

(79 pages)

PUBLIC ABSTRACT

The Effects of Froude Scaling on Velocity-Induced Vortices in Physical Models

The Utah Water Research Laboratory at Utah State University proposes to examine further a little known issue frequently seen in research conducted. The Utah Water Research Lab frequently conducts physical model studies of hydraulic structures for organizations around the world during the design process. These studies allow engineers to determine potential design revisions though simulations of operations including flood flows. Often, vortices, or whirlpools, occur in these models. Vortices are common occurrences at intakes in hydraulic structures such as dams and pump sumps. They can be detrimental to the operation and efficiency of these structures.

The purpose of this work is to examine the change in vortex behavior at differing physical model scales. This was done using four identical experiments built at differing scales with the largest of the four being defined as a prototype. Each experiment created vortex flow at the intake to a sluice gate using unique approach conditions.

This study contributes to the existing knowledge by providing a set of both qualitative and quantitative observations made from images in multiple perspectives and measured data. The study will allow researchers to understand better the relationships between observed vortices in physical models and predicted vortex behavior in the constructed prototype.

Michael S. Budge

ACKNOWLEDGMENTS

I would like to thank the Utah Water Research Laboratory and the faculty members there for their support. In particular I would like to thank my advisor, Steve Barfuss, who has given me the insight and direction to pursue this research. I appreciate Zac Sharp for his patience helping me through the construction and testing of the physical models. Thanks also to Ken Jewkes for allowing me to use his hydraulics lab and for his assistance. Gilberto Urroz has been an invaluable resource in researching theory and background. Thank you to my committee members, Dr. William Rahmeyer and Dr. Paul Barr, for their support as well.

Michael S. Budge

CONTENTS

LIST OF TABLES

LIST OF FIGURES

LIST OF SYMBOLS

B = width of channel

b = width of sluice gate

D_{Vn} = vortex diameter at free surface at location n

g = acceleration due to gravity

H = critical submergence

P = pressure

Q = discharge through sluice gate

r, φ, z = cylindrical coordinates

T_p = time of vortex presence

T = Temperature

r = radius of vortex

r_1 = radius of vortex region

V_a = approach channel velocity

V_t = tangential velocity

y_0 = piezometric head upstream of gate

y_g = sluice gate opening

Γ = circulation

ν = kinematic viscosity of the fluid

ρ = density of the fluid

σ = surface tension of the fluid

υ_r = tangential velocity component

υ_z = tangential velocity component

υ_θ = tangential velocity component

ω = angular velocity

CHAPTER I

INTRODUCTION

Purpose

Free surface vortices are regions within a fluid where the flow is rotating about an central axis that may be either straight or curved in vertical alignment. This highly organized flow phenomena can occur in fluid bodies near conduit intakes and can frequently be observed at obstructions to flow (Anwar 1965). For example, they can be seen in vertical and horizontal intakes, pumps, sluice gates, or in flow areas downstream of bridge support columns causing eddying and swirl. Vortices occurring at intakes can cause negative effects to the intake such as head loss, reduction of discharge, loss of efficiency, surging, vibration, or air entrainment (Gulliver and Rindels 1987). Further, air entrainment can cause mechanical damage to equipment in the form of cavitation, loss of efficiency, and suction of debris into the intake from the free surface. Considerable research has been undertaken to avoid the formation of vortices, including research using model studies.

Hydraulic scale models are often used as design tools (Odgaard 1986) and are being used successfully in a wide variety of situations. However, scaling criteria (and thus scale effects) are uncertain for vortex-flow phenomena despite considerable research efforts. It is the purpose of the present work to provide a simple, experimental, free-surface vortex model for the discussion of scale effects on velocity-induced vortices in open channel flow.

Hydraulic structures are typically designed to prevent the formation of such vortices to avoid the negative effects previously mentioned. Often, the use of physical hydraulic modeling is helpful in the design processes of many hydraulic structures. Such models, if designed properly, often operate under the principles of Froude similitude, which take into account forces due to gravity, inertia, and velocity. In the operation of physical models, the formation of vortices is frequently observed in areas where they would be expected (Hecker 1981). Although there has been a great deal of research performed to evaluate scale effects of vortices in static pools (Anwar 1965; Gordon 1970; Gulliver and Rindels 1987), there has been very little research performed to evaluate the scale effects associated with velocity induced vortices in physical models. None of the literature researched for this study examined vortex behavior across scaled Froude models of a prototype. Numerical modeling methods, including computational fluid dynamics (CFD), were not incorporated in this research. They could be used, however, in future work to further this analysis.

Differences between vortices in static pools and velocity-induced vortices will be explained further in Chapter III. The purpose then of this research is to examine how Froude scaling affects vortex formation in- physical models through a series of four identical experiments built at differing scales. The experiment consists of an adjustable sluice gate installed in an open channel with approach conditions designed to create approach swirl and vortex flow. Sketches of the experiment in plan and profile view are shown below in Figures 1 and 2.

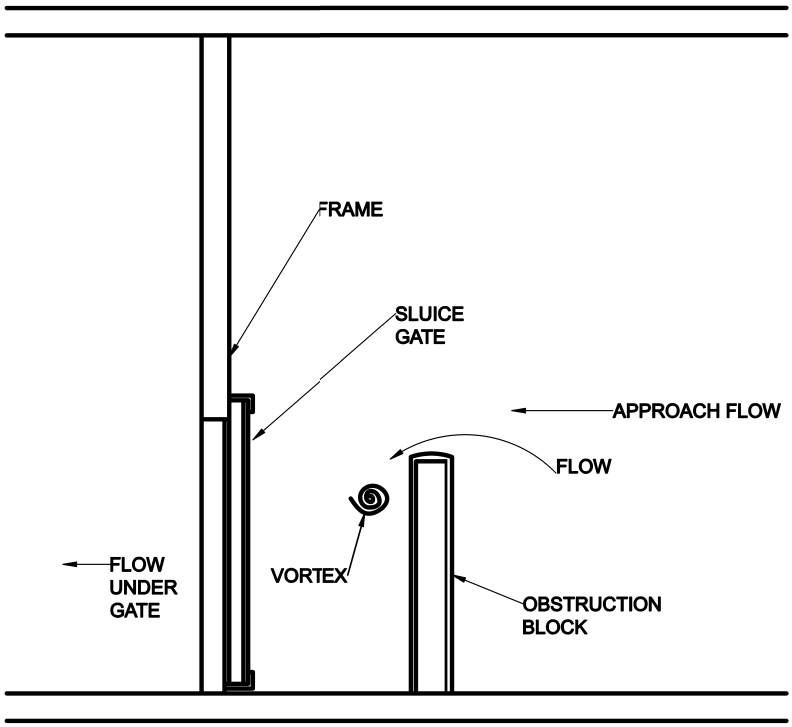

Figure 1. Sketch of test setup in plan view.

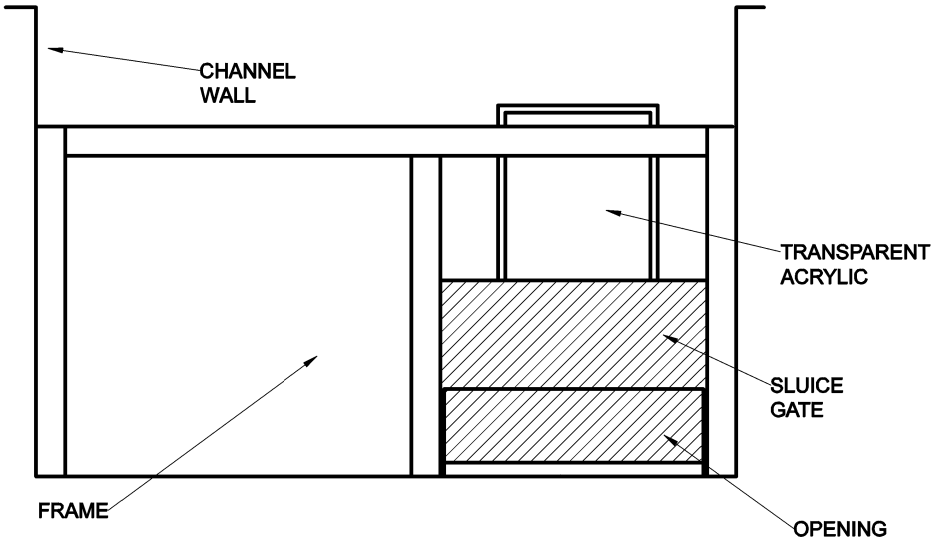

Figure 2. Sketch of setup in profile view looking upstream.

The largest of the four experiments will be called the prototype and the three others will be modeled after it. The four models were built at scales of 1:1, 1:1.98, 1:2.67, and 1:8. These scales were chosen based on the available equipment for experimentation. For consistency, these experiments will be defined as Model A, Model B, Model C, and Model D, respectively, with model A being the prototype. Models B, C, and D are each physically smaller than model A. These are explained in further detail in Chapter IV.

Objective

The main objective of the present work is to observe and quantify scale effects on the formation of free surface velocity-induced vortex formation. This is accomplished by conducting physical experiments, recording data, and organizing the results into relevant conclusions. These results are compared to previous studies on theories of vortex formation.

In the present work, a series of four hydraulic models of varying sizes were constructed using principles of Froude scaling in order to study the effects of scaling on the vortices. The largest of the four structures is defined as the prototype and three other structures are scale models of that prototype. These experiments are described in full detail in Chapter IV. This research takes a unique approach to the study of vortex scale effects through creation of multiple experiments that are geometrically similar to one another. This research contributes a set of observations of vortex formation and behavior across these differing model scales. The observations are presented both quantitatively and qualitatively through images and measured data.

The specific research components for this study include:

1. Conduct an experiment consisting of a sluice gate in an open channel flume that allows for the formation and observation of vortices induced by a wall set in the flow path immediately upstream of the sluice gate so that a separation forms.
2. Recreate the experiment at multiple geometrically smaller scales using Froude scaling principles.
3. Re-conduct the same procedures carried out during the initial experiment in the scaled models
4. Analyze results and draw conclusions

The resulting data is expected to give a strong correlation between model scale and vortex behavior within the model. This thesis reports on trends in the observed data and makes appropriate conclusions based on the observations.

Outline

Chapter I lays out an introduction to the subject matter while providing a need for the research that is undertaken. Chapter II reviews previous study and literature published on vortex-flow and scale effects. Chapter III gives background on both free surface vortex-flow and Froude scaling. Chapter IV explains the methods used in this research to model scaling effects on velocity-induced vortices and Chapter V gives the experimental results. Discussion and conclusions are found in Chapter VI, which includes an in-depth observation and analysis of trends. References are then listed with the appendices following.

CHAPTER II

LITERATURE REVIEW

Heimholtz Vortex Theorems

Hermann von Helmholtz published studies on the behavior of vortices in inviscid fluid as early as 1858 at the University of Königsberg in Berlin. In his paper, Hermholtz established three theories of vortex motion. These theorems, which are applicable for understanding the nature of vorticity and vortex flow, are translated from the German and appear in a textbook by Schobeiri (2010). Heimholtz stated in his first theorem that "a vortex line is, at any particular time, a curve which has the same direction as the velocity vector,

$$\overline{\Omega} = \Delta\Lambda\, \overline{V} \tag{1}$$

where $\overline{\Omega}$ is the vorticity vector and $\overline{V}$ is the velocity vector at each point of the line." Mathematically, vorticity is a vector, defined as a curl of the velocity field and the vortex line is tangential to the vorticity vector at all points along its length (Kivineimi and Makusa 2009).

The second Heimholtz theorem states that "the fluid elements that lie on a vortex line at some instant continue to lie on a vortex line, i.e. the vortex lines move with the fluid." This is shown in Figure 3.

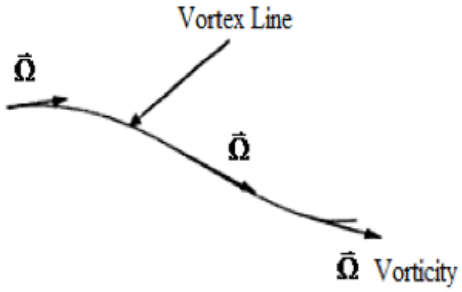

Figure 3. Vorticity along a vortex line (Kivineimi and Makusa 2009)

The theorem states that vorticity on a surface S is defined as,

$$\Omega = 2\omega \tag{2}$$

where ω = angular velocity (rad/s). The third theorem states that "the quantity

$$\Gamma = \int_s \ \omega n dS \tag{3}$$

is the same for all cross sections S of a vortex tube." Which can be solved giving,

$$\Gamma = 2\pi\omega r_1^2 \tag{4}$$

where Γ =circulation and r_1 is the core radius and r is the radius of free vortex.

Contemporary Research

The studies discussed in this section have all examined vortices that form in static pools or have been artificially induced in controlled laboratory situations. This research differs from these studies by looking specifically at velocity-induced vortices as opposed to vortices formed though the Coriolis force, among others. The present study has been

designed with specific approach geometry to examine velocity-induced vortices because little research has been completed on this subject to date.

Anwar (1965, 1967, and 1968) conducted a number of theoretical and experimental studies of flow conditions in strong steady vortices with an air core forming at the intake of a pipe from a cylindrical tank. The tank was initially static and rotation induced from jets in the sidewalls of the cylinder. The conditions for the formation of an open vortex with an air core at the intake and the condition of similarity between vortices of differing scales were discussed. They found that model studies are effective tools to use to examine vortices and recommended a relatively large scale such as 1:20. It was also shown that vortex formation depends on the depth of submergence and the swirl in the oncoming approach flow. The work presented methods of predicting vortices at intakes and calculating swirl at intakes. It was reported that intake efficiency was improved by using a floating object on the surface directly above the intake and by diffuser walls to dissipate energy by providing extra roughness.

Gordon (1970) described the development of design criteria to avoid vortices at low-head intakes, based on a study of 29 existing full-scale hydroelectric intakes in reservoirs. All of the vortices observed in this study were in static reservoir pools and were generated by the intake flow into penstocks along with local approach geometry. The study proposed that the formation of vortices depended on the critical submergence (H), velocity at the intake, size of the intake, and the shape of the approach area. Although he did not attempt to examine or measure the vortices that formed, Gordon proposed a relationship for critical submergence to avoid vortex formation. The

relationship is given as

$$H = kVD^{1/2} \quad (5)$$

where H is the critical submergence level required to prevent air-entraining vortex formation (ft), D is intake diameter (ft), V is average velocity (fps), and k =0.3 for symmetrical and 0.4 for unsymmetrical approach flow.

Investigation conducted by Anwar et al (1978) on the onset of air-entraining vortices at a horizontal intake showed that flow conditions in an air-entraining vortex are not affected by surface tension and viscosity of the test fluid when radial Reynolds number and Weber number are larger than 3 x 10^4 and 10^4 respectively. Experiments were conducted with a circular intake in the side of a channel with no obstructions in it. It was shown that bell mouth entries do not improve critical submergence heads as compared with a simple pipe intake. In the case of an intake with and without bell mouth and mounted flush with sidewall of the flume, it was noted that the boundary wall reduces circulation and thus the critical submergence to a point that the water surface almost reaches the intake lip before air-entraining vortices occur.

Padmanabhan and Hecker (1984) conducted experiments using one full sized and two reduced-scale models of a pump sump to geometric scales of 1:2 and 1:4 to determine whether scale effects distort the predictive ability of hydraulic models of pump sums with large scale ratios. Possible scale effects on vortex formation, swirl, intake losses, and air ingestion due to air-entraining vortices were examined using the experimental results. It was found in this particular study that no significant scale effects on modeling free-surface vortex formation occurred in the 1:2 and 1:4 models operating according to

Froude similitude. Also, some limited measurement of angular velocity away from the vortex core indicated good scaling of angular velocity by the models. They also concluded that for model pipe Reynolds numbers above 1 X 10^5, the full-scale intake losses were predicted well by the reduced scale models. For R_e below 1 X 10^5, some Reynolds number effects are possible, since higher loss coefficients were indicated by the reduced scale models. However, this study looked at vortices that formed in a static pool with sump intakes at the floor of the pool. They did not look at velocity-induced vortices that are influenced by approach geometry.

Odgaard (1986) studied a Rankine vortex model as a basis for an equation for critical submergence of intakes. He defined critical submergence as the depth of incipient air entrainment or the depth at which the depth of the vortex air core reaches the intake. The equations presented related critical submergence to Froude number, circulation number, Reynolds number, and Weber number. He found that Froude and circulation numbers were the major controlling parameters. Experimental data corroborated this theory by comparing measured and computed critical submergences plotted against Froude number. It was concluded that the orientation of the intake may have little effect on the criteria for air-entrainment in vortices.

Gulliver and Rindels (1987) studied weak free surface vortices at vertical intakes. They defined a vortex as a result of angular momentum conservation at the flow constriction where angular velocity increases with the decrease of cross sectional area. Hite and Mih (1994) derived concise equations for tangential, axial, and radial velocities as well as the water surface profiles of air-core vortices. Experiments were performed

that indicated that the derived equations agreed with measurements and are applicable to vortex motion. Radial velocity was here derived as:

$$v_r = -v_e \frac{8r}{r_m^2+2r^2} = \frac{v_e}{r_m} \frac{8\bar{r}}{1+2\bar{r}^2} \quad (6)$$

where r =radius and v_e = eddy viscosity, r_m= core radius, and $\bar{r}$ = r/r_m. It was reported that in high Reynolds number flow, the eddy viscosity could be several thousand times larger than the kinematic viscosity.

Yildirim and Kocabaş (1995) examined how approach-flow boundaries affect critical submergence for intakes in open channel flow. They examined multiple intake approach geometries in their paper to document their effects on vortex formation, which makes their research fairly similar to the present work. The paper summarized the significant effects of the Reynolds number and the Weber number in their literature review as follows. Jain et al. (1978) have shown that surface tension may be important for vortices with low circulation. The experimental study of Jain et al. (1978) infers that within the range of $120 < W_e < 10^4$ the surface tension does not affect vortex formation. Odgaard (1986) has shown that for the case of air-entraining vortices in a still body for $W_e < 720$ and $R_e > 1.1 \text{ X } 10^5$, the effects of surface tension and viscosity can be neglected, respectively. Padmanabhan and Hecker (1984) give $W_e > 600$ and $R_e > 7.7 \text{ X } 10^4$ for neglecting the respective surface tension and viscosity effects.

Gürbüzdal (2009) researched scale effects on the formation of vortices at intake structures. A series of experiments were conducted on four intake pipes of differing diameters located in a large reservoir. Although similar, this research differed from the

present work in that the reservoir size remains constant across the series of experiments. The relationship of critical submergence ratio with other dimensionless parameters was considered for a given Froude number. It was found that the critical submergence ratio was affected by model length scale ratio and Reynolds number differences between model and prototypes. In addition to this, the Reynolds number limit, beyond which viscous forces do not affect the vortex flow, is found to increase with the increase of Froude number. An empirical relationship, which gives the critical submergence ratio as a function of Froude number, sidewall clearance ratio and Reynolds number was obtained by using data collected in his experiments.

Kivineimi and Makusa (2009) prepared a master's thesis on a scale model investigation of free surface vortex with particle tracking velocimetry. In their study, the formation of free surface vortex and the affecting factors on its strength were studied at spillway intakes of 1:100 hydraulic scale model of Xiluodu hydropower dam in China. The findings presented reflected the true behavior of vortices in the prototype. Since the prototype has not yet been built in this case and it is yet unknown if vortices formed, it is unclear from this study if vortices are accurately scalable at models of this scale. Data collection was done using particle tracking velocimetry (PTV) on the free surface flow field around the spillway intakes of the dam. The surface flow field data produced by the PTV system was interpolated, and the obtained full flow fields were analyzed according to the Helmholtz vortex theorems and Rankine combined vortex theory principles; velocities around irregularly shaped vortices were averaged and the circulation strengths were calculated according to the theory.

CHAPTER III

BACKGROUND: VORTICES AND FROUDE SCALING

Vortex Theory

The formation of vortices is the result of a complex set of physical interactions between the intake geometry, approach area, velocity profiles, and the properties of the fluid such as surface tension and viscosity. Since flow into various intake structures is similarly complex, the design of many such intakes rely on model studies to avoid these damaging vortices (Gürbüzdal 2009).

Approach conditions have a large factor on the formation of vortices. Many of the intake geometry conditions like those shown in Figures 4 and 5, induce swirl and vorticity to the flow due to the way the channel affects velocity patterns. Vortices can also form in static pools without the influence of velocity. A static pool is defined as an approach area that has negligible approach velocity, which can be the largest source of swirl leading to vortex formation. In cases such as these, vortex flow occurs due to the Coriolis effect, which originates from the rotational forces of the Earth rotating on its axis. Shapiro (1962) performed an experiment with a completely still body of fluid. The stop on a small pipe intake on the bottom of the container was removed and after 15-20 minutes, rotational velocity was observed in the body of fluid. Analysis of the results showed that the rotation is indeed due to the Coriolis force. In the southern hemisphere, rotation will be in the clockwise direction and counter-clockwise in the northern hemisphere (Shapiro 1962). Such forces, however, are weak, and are generally

observable when no other forces are acting on the flow. Other forces have greater influence on drain direction. This study does not examine vortices in static pools because it specifically looks at velocity-induced vortices. The approach conditions in these experiments differ from static pool conditions because the primary source of swirl and rotation is from the velocity resulting from the fluid interacting with the approach geometry.

In hydraulic structures, there are numerous causes of swirl that, when strong enough, may lead to vortex formation. The difference between vortex formation in static pools and through asymmetric approach conditions is due to the presence of velocity in the approach area flow. Theoretically in a very long, wide, symmetrical channel without rough sides, all the forces affecting the flow and creating swirl are so balanced and weak that no swirl occurs. In more typical applications, water may move along bends and through small gaps with supercritical velocities where swirling motion is created around the asymmetrical areas in the flow (Kivineimi and Makusa 2009). Figure 4 shows various types of vortex formation associated with asymmetry.

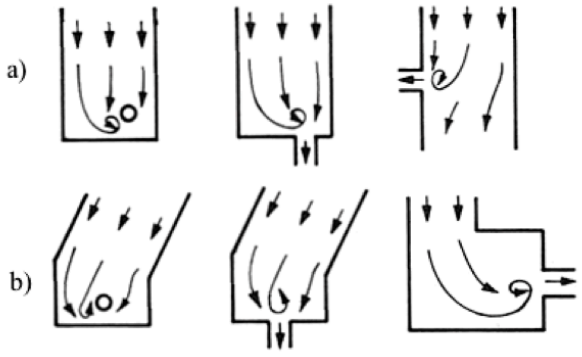

Figure 4. Rotational flow arising from a) asymmetry and b) change in direction of boundaries (Knauss, 1987)

In addition to swirl sources, there are other structure-related sources. Figure 5 illustrates some of these cases (Knauss 1987). Cases a) and b) in Figure 5 are types of asymmetric conditions. Although swirling by velocity gradients (case b) can also be initialized by the Coriolis force (Shapiro 1962) the direction of swirl is usually a decided by asymmetric geometry or flow conditions (Kivineimi and Makusa 2009). Intakes may create vortex-formation whether the intake is located on the floor or walls of the basin, or if it is projecting into the fluid body.

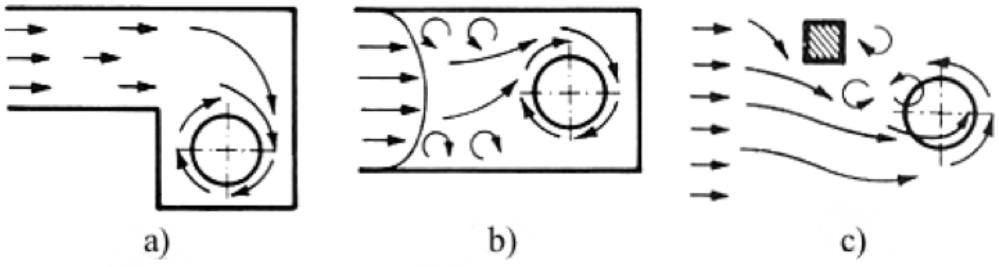

Figure 5. Sources of vorticity: a) offset introduction, b) velocity gradients, and c) obstruction. (Knauss 1987)

Vortices form under many differing intake arrangements. Figure 6 illustrates the different classifications of intakes based on these distinctions.

Besides the multitude of arrangements in which vortices form, the strength of the vortex can also be classified. Since reliable measurement is often not easily accomplished, the most effective method of determining these classifications is by visual observation. Quantitative distinctions have not been made between these types. However, in a qualitative sense for example, observation of a dimple in the surface demonstrates the presence of a stronger vortex than simply the presence coherent surface swirl. Alden Research Laboratory in Massachusetts (Hecker 1981) developed a guideline

to provide a consistent means of classification. A visual classification of vortices consists of the following types, shown visually in Figure 7 (Knauss 1987). Although these guidelines provide differentiation of types, vortices often form intermittently. For example, a vortex is identified as a type 6 if it exhibits at least a full air core intermittently among other observed conditions.

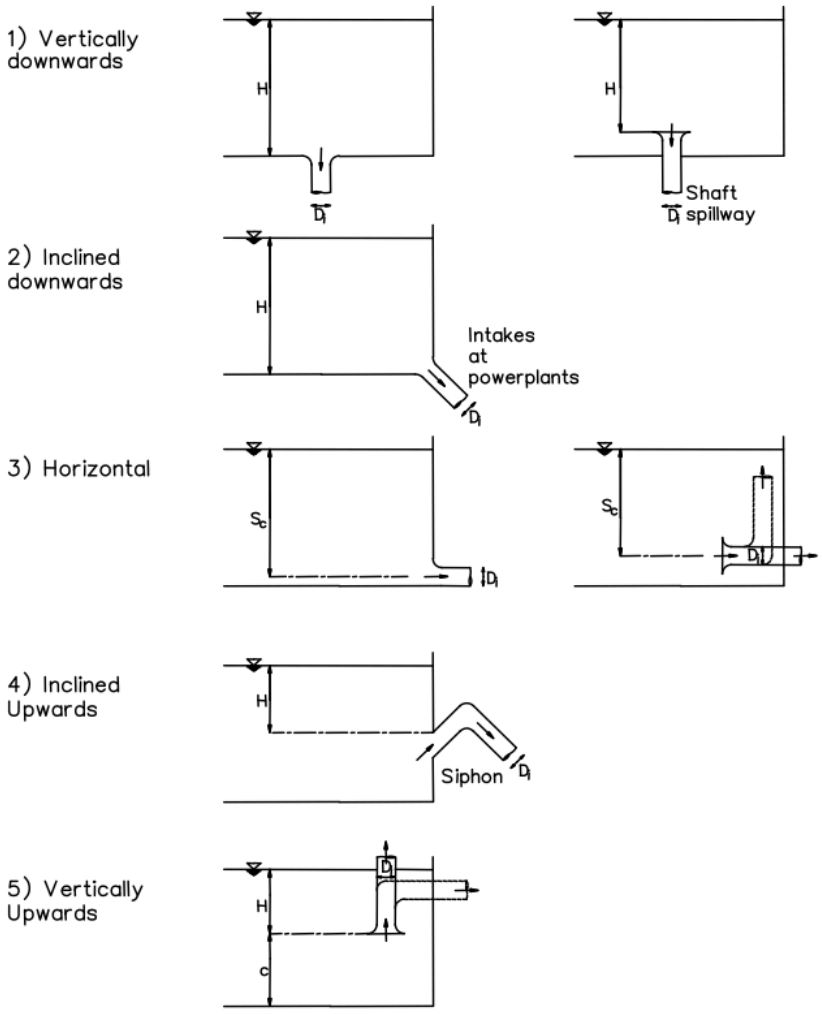

Figure 6. Directional and structural classification of vortices (Knauss 1987)

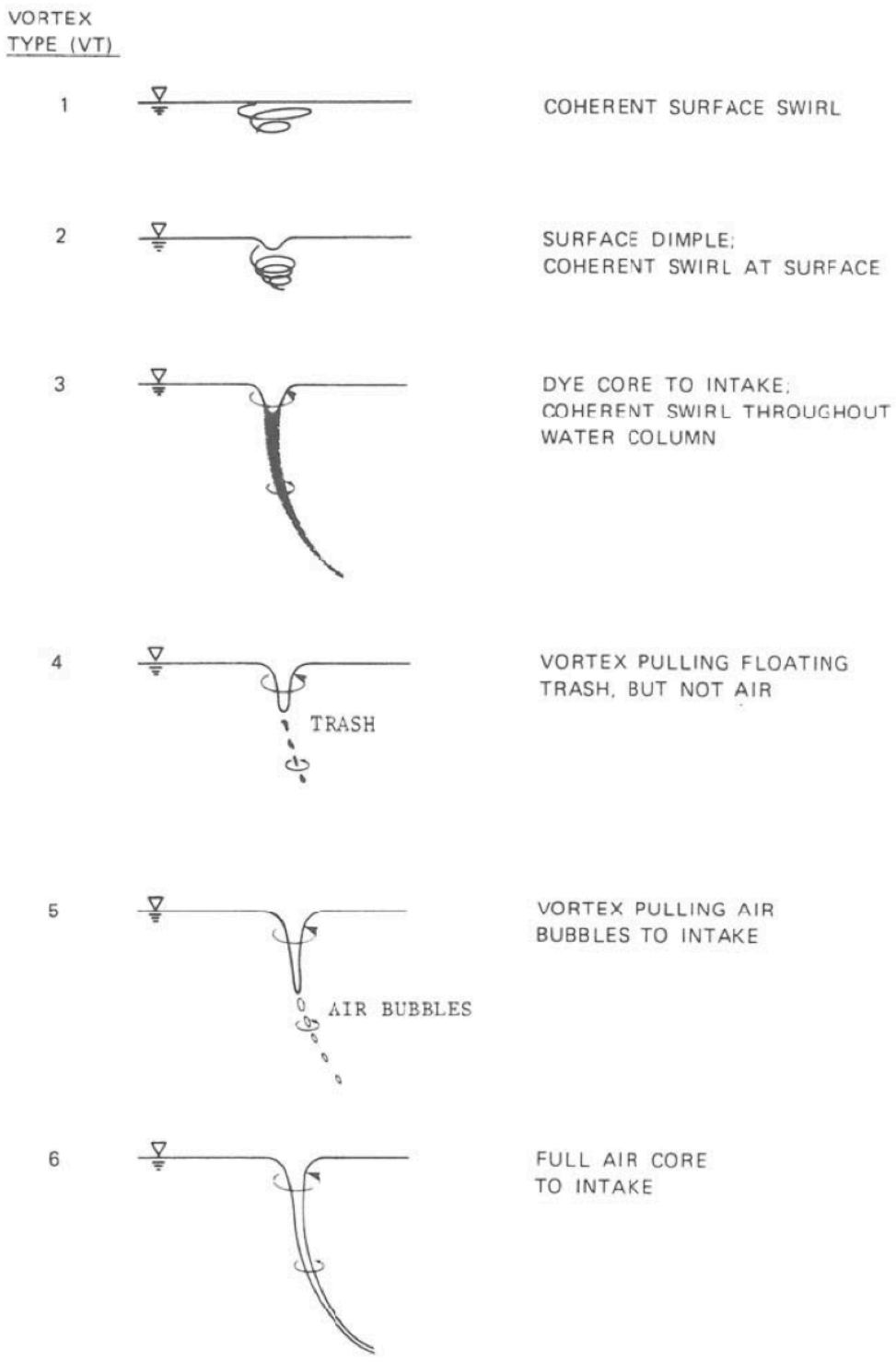

Figure 7. Vortex type classification (Knauss 1987)

1. A type 1 vortex is weakly developed with no air core and only a small eddy on the water surface indicating presence of the vortex.
2. A type 2 vortex exhibits coherent surface swirl that will turn into a small depression on the free surface.
3. A type 3 vortex has a non-air-entraining tail and air bubbles are not drawn into the intake from the surface. Dye placed in the vortex tail is carried downward into the intake forming a filament that reveals the location of the vortex axis.
4. Type 4 vortices are strong enough to ingest more buoyant particles such as floating trash on the surface but not air.
5. A type 5 partially developed air-entraining vortex does not have a continuous air core. The air core extends only part way down from the water surface and ends with a vortex tail. Occasionally, small bubbles may be dragged from the vortex tail down the longitudinal axis of the vortex to the intake.
6. A type 6 fully developed air-entraining vortex has an air core extending from the water surface into the intake. Near the water surface the air core has a funnel shape and below the water surface a rope-like appearance. Because of the heavy entrainment of air and the negative effects that causes, formation of this vortex type at intakes is adverse or unacceptable.

The Rankine combined vortex theory expresses the theoretical between vortex shape and swirl parameter (Kivineimi and Makusa 2009). In the central region of the vortex, the fluid is assumed to rotate so that the tangential velocity,

$$V_t = \frac{(\#rev)\pi D_{V1}}{t} \tag{7}$$

where ω = angular velocity (rad/s) (Knauss 1987) and varies linearly with r (Kivimini and Makusa 2009). This parameter will be used in the analysis.

Froude Scaling

For physical models to properly simulate hydraulic conditions in the prototype, dynamic, kinematic, and geometric similarity are required. Geometric similarity occurs by maintaining all linear dimensions under the same scale ratio (Finnemore and Franzini 2002). Kinematic and dynamic similitude involves contributions of forces in the fluid flow including inertia forces, viscous forces, gravitational forces, pressure forces, elastic forces in the fluid (compressibility), and surface tension forces. Many hydraulic models are modeled using Froude scaling, which is based on the ratio of inertia to gravity forces. This principle is based on the Froude number, which is defined as:

$$F_r = \frac{V}{\sqrt{gy}} \tag{8}$$

where V is a characteristic velocity, g is the gravitational acceleration constant, and y is a characteristic linear dimension. In the case of each dimensionless parameter in this study, the characteristic velocity is the velocity under the sluice gate. Similitude occurs when the Froude number in the prototype matches the Froude number in the model, which ensures that the above-mentioned forces are scaled properly (Finnemore and Franzini 2002). Parameters including length, head, pressure, velocity, discharge, and time can be calculated for the scale using the following equations derived from the Froude number. The length ratio is defined as $1{:}L_r$ where L_r is the scale.

$$Length{:}\ L_p = L_r L_m \tag{9}$$

$$Head:\ H_p = L_r H_m \tag{10}$$

$$P\square essure:\ P_p = L_r P_m \tag{11}$$

$$Velocity:\ V_p = {L_r}^{0.5} V_m \tag{12}$$

$$Discharge:\ Q_p = {L_r}^{2.5} Q_m \tag{13}$$

$$Time:\ T_p = {L_r}^{0.5} T_m \tag{14}$$

Dimensionless Parameters

Based on the theory of dimensional analysis, the following parameters apply for the scope of this study. In literature, almost all researchers considered the effects of these parameters on formation of vortices. Since it is difficult to achieve similarity of each of these parameters across the models, a discussion of their relative importance is as follows. Equations 15-18 define the dimensionless parameters calculated in this research.

Weber Number

$$W_e = Weber\ Number = \frac{V}{\sqrt{\sigma/\rho D}} \tag{15}$$

Here, σ is surface tension and ρ is density (Finnemore and Franzini 2002). The Weber number is basically effective in weak vortices that only exhibit a surface dimple. As it was stated in the researches of Jain et al. (1978), Gulliver and Rindels (1987), and others, surface tension effect can be neglected in practice of air-entraining vortices.

Reynolds Number

$$R_e = Reynolds\ Number = \frac{VD}{\nu} \tag{16}$$

In literature, almost all researchers considered the effect of viscosity on the formation of vortices and determined limits of Reynolds number beyond which viscous forces are negligible according to their own experimental results. Therefore the influence of Reynolds number for this study was taken into account. In this study, Reynolds numbers are calculated and reported in Chapter V. However, Reynolds number effects were not looked at in this research.

Froude Number

Almost all research conducted on vortex flow, with exception of Yildirim and Kocabaş (1995), have indicated Froude number (Equation 8) to be among the important parameters influencing critical submergence. This is expected because it is a free surface phenomenon and affected by gravity (Gürbüzdal 2009). Hence, it is expected to base the model study of vortex formation on Froude number similarity.

Elkman Number

This dimensionless parameter is defined as

$$E_k = Elkman\ Number = \frac{\nu}{\omega D^2} \tag{17}$$

where ν = kinematic viscosity, ω = angular velocity, and D = a linear dimension such as diameter (Liggett 1994). This parameter deals with rotating flow with viscous (turbulent) terms and rotational terms.

CHAPTER IV

EXPERIMENTAL METHODS

Experimental Setup

The present experimental research consists of a single experiment repeated four times at differing scales. The largest experiment was the prototype and was labeled Model A. The smaller Models B, C, and D were created at smaller scale ratios. In a long, rectangular open channel, a transparent acrylic frame was placed across the width of the flume that included an adjustable sluice gate on the right hand side looking upstream. A transparent acrylic gate was installed over the opening with guides allowing vertical movement to create a structure similar to a sluice gate.

In order to produce uniform approach flow free of surface waves and turbulence, a diffuser screen was installed in the channel a length of ten channel-widths upstream of the gate. This enabled water to enter the experimental area smoothly and allowed for formation of stable vortices without disruptive surface disturbances. An obstruction block of the same height as the frame and extending roughly 1/3 of the width across the channel and immediately upstream of the sluice gate opening was fastened to the channel wall ¼ of the channel width upstream of the sluice gate to cause an obstruction in the flow. This created enough swirl to encourage formation of a velocity-induced vortex.

The diffuser wall was included in the experiment also had the purpose of creating a uniform flow profile. This uniform flow profile could not be achieved in the approach channel without this diffuser wall, which was constructed from air conditioning mesh

attached to a metal grating. Near uniform conditions were achieved once this was installed.

Figure 8 shows the test schematic for Model A in the 8 ft. flume. Designs for each of the smaller scaled experiments were created to be geometrically similar to the prototype experiment. Note the arrow in Figure 8 that points to what will be referred to as the obstruction block. Table 1 contains a summary of important dimensions and parameters for all four experiments. Dimensions were scaled down from the prototype using Equation 9, with discharge scaled using Equation 13, and velocity scaled with Equation 12. Twelve total flow rates were used across all the models. They are notated as Q1, Q2, and Q3 with the subscripts A, B, C, and D denoting the model scale in which they occur. Q1A was defined as the flow rate at which a type 6 vortex was found to form in model A. Q2A was the flow rate at which a type 5 vortex was found to form in model A. Q3A was the flow rate at which a type 5 vortex was found to form in model A. In the other models, they are the Froude scaled flow rates.

Length ratios are shown in Table 1 as well. The length ratio is defined as the ratio of a characteristic length in the prototype to the same characteristic length in the prototype as given in Equation 9. For instance, the width of the flume in Model B was 4.02 feet and therefore the length ratio is 8/4.02, which is a ratio of 1.98. In other words, the model size and model length ratio are inversely proportional.

Table 1. Summary of experimental parameters across scales.

Model	Flume Width (ft)	Length Ratio	Flow Condition	Discharge (gpm)	Approach Velocity (fps)	Sluice Gate Opening (in)
A	8.0	1	Q1A	2387.8	0.19	1.63
A	8.0	1	Q2A	1943.4	0.14	1.00
A	8.0	1	Q3A	1746.0	0.04	0.75
B	4.02	1.98	Q1B	432.8	0.13	0.82
B	4.02	1.98	Q2B	352.3	0.10	0.51
B	4.02	1.98	Q3B	316.5	0.09	0.26
C	3.06	2.61	Q1C	205.6	0.11	0.61
C	3.06	2.61	Q2C	167.4	0.03	0.38
C	3.06	2.61	Q3C	150.4	0.02	0.28
D	1.0	8	Q1D	13.2	0.05	0.20
D	1.0	8	Q2D	10.7	0.02	0.13
D	1.0	8	Q3D	9.6	0.01	0.09

These geometrically similar experiments of model A in the 8-ft wide flume were constructed individually in separate open channels flumes. Model B was built in a 4-foot wide flume, model C built in a 3-foot wide flume, and model D built in a 1-foot wide flume. Each of these experiments was constructed in the Utah Water Research Laboratory or the Engineering Hydraulics Laboratory, both on the campus of Utah State University. In all but the 1-foot channel, flow was supplied with water from the Logan River from a large reservoir upstream of the laboratory and was discharged back into the river. In the 1-foot channel, a pump supplied flow where it ran into a sump to be recirculated. Figures 9-12 show photos of each experiment installed in their respective flumes.

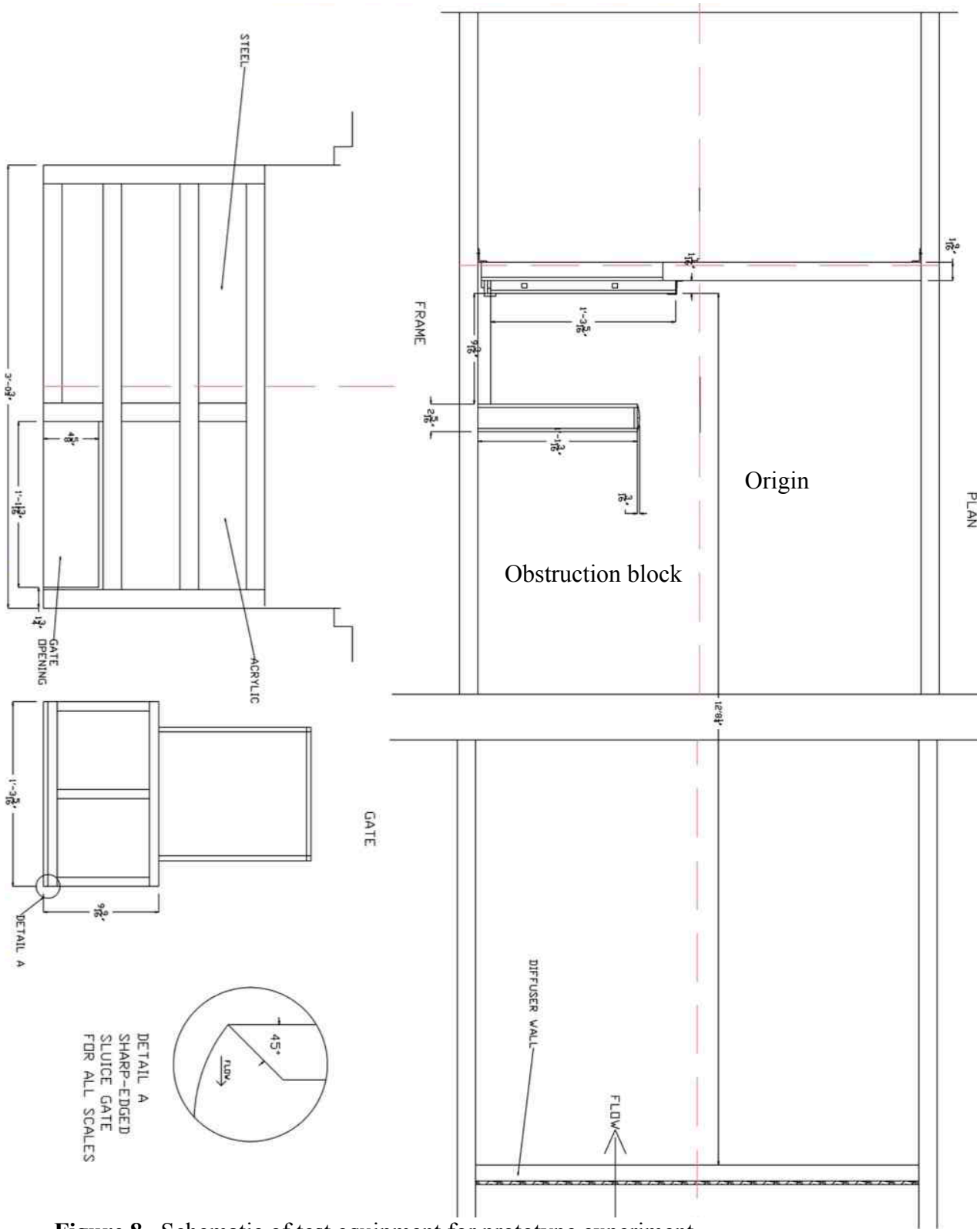

Figure 8. Schematic of test equipment for prototype experiment.

Figure 9. Model A prototype structure installed in 8-foot flume (looking upstream).

Figure 10. Model B experiment model installed in 4-foot flume.

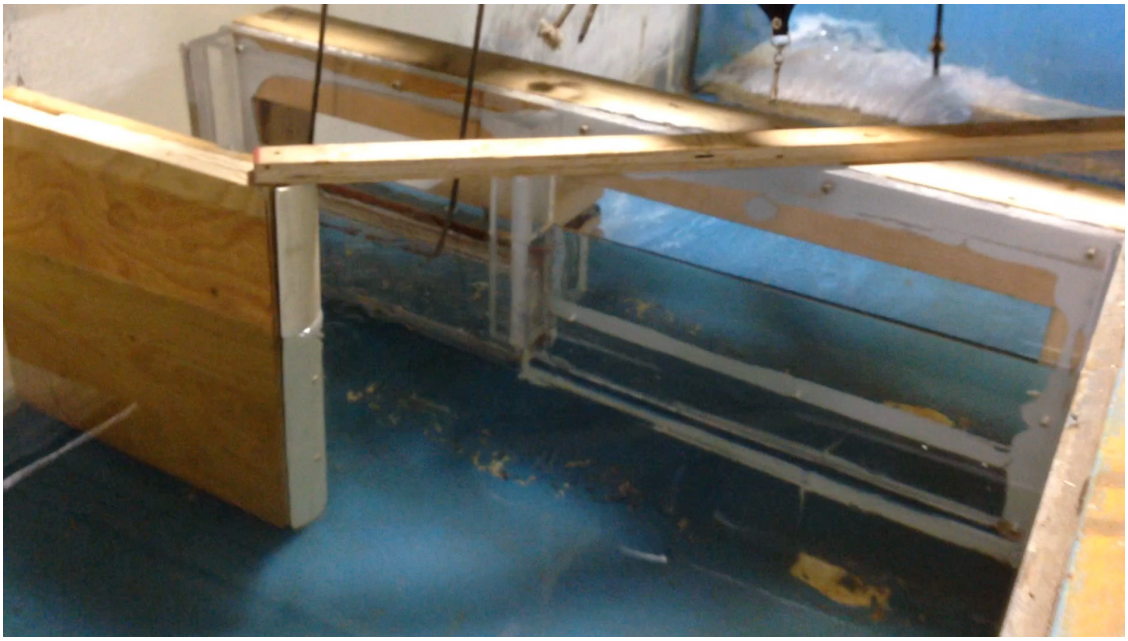

Figure 11. Model C experiment installed in 3-foot flume.

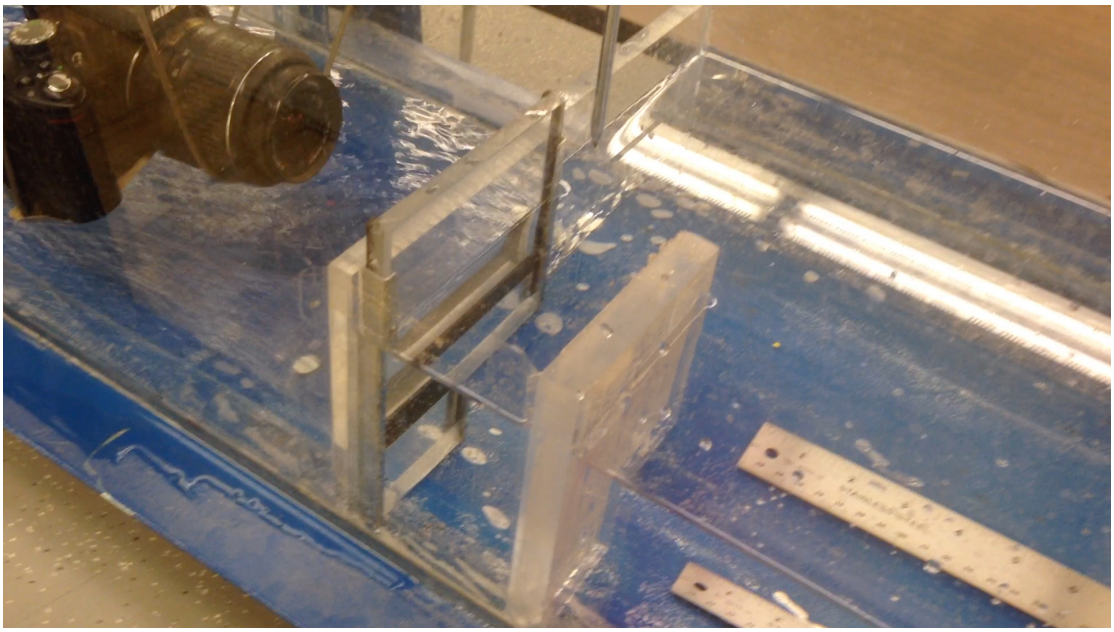

Figure 12. Model D experiment installed in 1-foot flume.

In addition to the video and photo observations made during the tests, the following data observations were made: flow rate (gpm), approach velocity (fps), upstream water depth (ft), gate opening (in), temperature (°F), vortex type, and time of presence. Time of presence is here defined as an indicator of the stability of vortex formation and is a ratio of time the vortex was present over an arbitrary recorded time. Head measurements were taken with point gauges with accuracies up to 0.01 inch in each experiment besides the largest. In the largest experiment, depth was measured with a measuring tape attached to the sidewall of the flume. Measurements of water depth and approach velocity were made in the same location across the experiments. In the prototype structure, this location was one foot directly upstream of the obstruction block at the centermost point of the block.

Photos and video observations of all vortices were made from two perspectives (profile and plan view) to aid in observation of vortex behavior, data recording, and documentation. Vortex location, diameter, and tangential velocity were determined using the photos and videos. A two-camera system was set up to make observations of the experimental area. A video camera was attached to a platform directly above the sluice-gate and a second camera was mounted at a specified location downstream of the gate. The transparent wall and gate allowed for clear profile images of the vortices to be taken against the backdrop of the obstruction block (Figure 8).

Procedure

A description of the procedure for model A is described here. The procedures of each of the other models are similar to the procedure for model A. After installation of the

gate structure and the diffuser wall in each of the respective flumes, the area upstream of the experimental area was filled to a water level near the top of the gate structure. The valve on the intake pipe was opened to begin flow into the flume and the sluice gate was opened to an arbitrary level. In the 8, 4, 3, and 1-foot flumes, flow was measured with a 24-inch Venturi meter, a 8-inch orifice plate, a 4-inch orifice plate, and a 2-inch orifice plate, respectively. By adjusting the sluice gate opening and the supply valve opening, a constant water level was achieved, which often took up to 45 minutes to stabilize. This process of adjustment continued until the presence of swirl, dimples, and vortex-flow were observed.

It should be noted at this point that channel approach velocities for each experiment, as shown in Table 1, were significantly low. This is seemingly contradictory with the premise of studying velocity-induced vortices. However, in the process of adjustment to achieve stable vortex flow, it was necessary to close the sluice gate and reduce the flow to the reported levels. Initially, discharges were greater and gate openings larger, but these higher approach velocities created heavy turbulence in the approach area and made it difficult to achieve formation of stable air-entraining vortices

This process was repeated to achieve the formation of the following three types of vortex in each of the four physical models:

1. Full air core to the gate opening (Type 6 as earlier defined).
2. Vortex pulling air bubbles to the opening (Type 5).
3. Vortex pulling floating debris to the opening but not air (Type 4).

The conditions that allowed for the stable formation of these vortices are referred to herein as Q1, Q2, and Q3 for each one of the types listed above, respectively.

Upon completion of data collection in model A, the same experimental procedure was followed for models B, C, and D. The values for discharge and gate opening had been established previously in model A. For each of the three flow conditions, the flow rate was properly scaled to match the length ratio of each smaller model. Similarly, gate opening, and camera positions were scaled to match previous conditions.

Scaling the prototype conditions to the model scale conditions required matching a combination of three parameters: discharge, gate opening, and upstream head. Once the Froude scaled flow rate was set, the gate was adjusted to the scaled prototype position. Due to uncertainties such as leakage in the flume structure, the gate required small adjustments from this point for the upstream depth to be scaled properly. In other words, upstream head and discharge governed the scaling from the prototype.

Observations were made in the same manner on vortex formation and behavior for each of the established conditions that induced the three vortex types observed in model A. Figures 13 and 14 show the setup for camera mounts behind and above the gate, respectively.

Once steady state conditions were observed, video and photographic observations were then made. In order to obtain accurate measurements from the observations, video from a plan view was taken simultaneously with profile photographs taken behind the sluice gate.

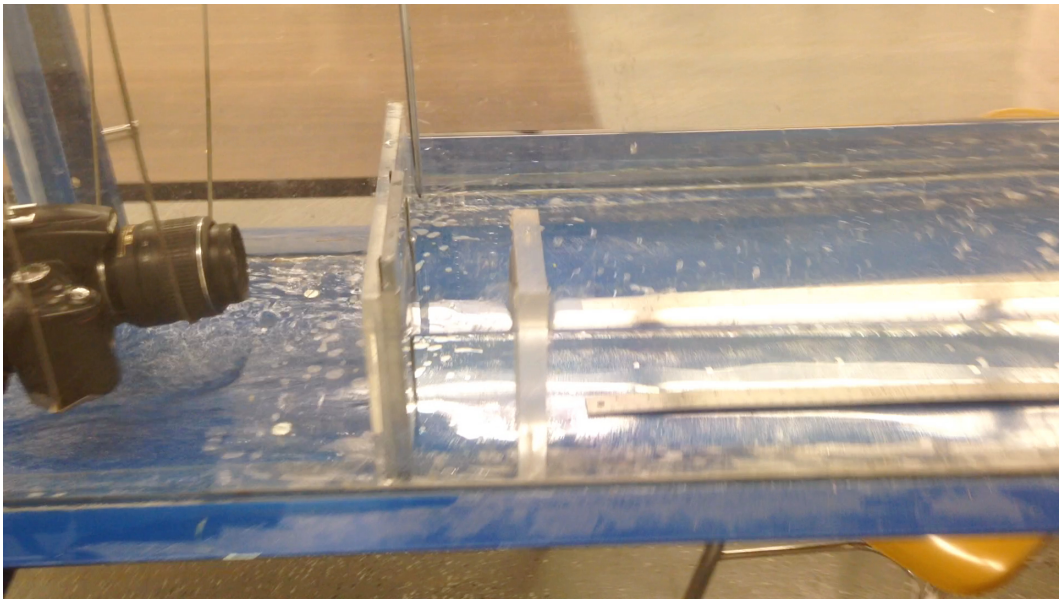

Figure 13. Camera mount for profile photos in model D.

Figure 14. Camera mount for overhead video recording installed in model B.

This was achieved by taking note of the elapsed video time the photograph was taken and extracting a still image from the video at that recorded time, allowing both images to show the vortex at the same moment in time. A coordinate system was established to record vortex occurrence locations in plan view with the origin at the point of the block closest to the center of the gate frame. Due to the often erratic and unstable nature of the vortex flow, steady and constant formation was frequently not observed. To account for this, three separate observation runs were recorded for each of the three flow conditions observed for a total of nine data runs for each scale. Averages were calculated for each of the three data runs within flow conditions.

Lengths were calculated by measuring pixels in the digital images using image analysis software. A ratio of pixels to actual length was obtained for each photograph by taking a photograph of a measuring tape in the exact location of the desired measurement, as shown in Figure 15 and Figure 16.

Once accurate length measurements were made from the overhead view, the distance from the vortex center to the block wall visible in the profile view was measured. A series of reference photographs with a visible measurement tape were taken with the tape at specified intervals. This enabled the creation of a table that could be used to obtain the correct pixel-length relationship for the precise location of the vortex in each photo. Pixel-length ratio values in between the specified intervals were linearly interpolated. These ratios were used to measure vortex diameter in profile view at three arbitrary locations in each instance.

Figure 15. Example of measurement method in model C. The photo is looking downwareds at the area between the sluice gate and obstruction block with the upstream direction pointing upwards.

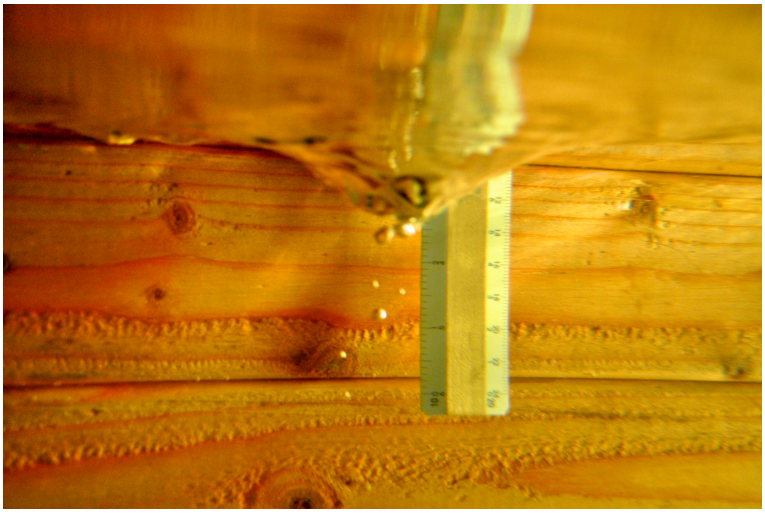

Figure 16. An example of measurement method in profile view in model B. This photo was taken from behind the downstream side of the sluice gate looking upstream at the obstruction block in the background.

The largest measurement (D_{V1}) was chosen as the distance from where the aerated vortex core begins to form near the free surface. This measurement was compared with the measurement of the same dimension from above. It was observed that the slope of the air core changed significantly in nearly every photo taken. Therefore, this point of slope tangency was chosen as the location of the measurement of D_{V2}. D_{V3} was chosen 1.5 inches below the second location in model A. In the smaller models, the location of D_{V3} was chosen as a scaled down distance from the second location. For example, in model B, D_{V3} was measured 0.76 inches below the D_{V2}. In many instances, the air core did not extend deep enough to measure at D_{V3}. These locations are shown visually in Figure 17.

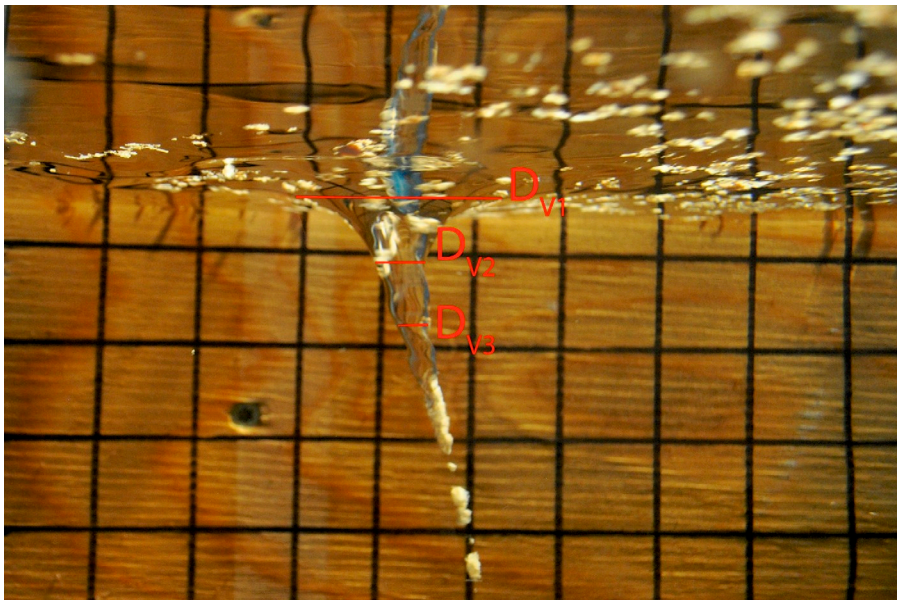

Figure 17. A Type 5 Vortex in model C shown with the locations of measurements D_{V1}, D_{V2}, and D_{V3}. This photo was taken from behind the downstream side of the sluice gate looking upstream at the obstruction block in the background.

Tangential velocity was estimated by analyzing the videos from above at reduced speeds. At the beginning of each data run, small particles were placed on the water surface upstream of the sluice gate to represent floating trash on the surface. The particles allowed flow paths in the vortex-flow and approach to be highlighted clearly in the video. Rotations over a given time period about the axis of the vortex in the video were carefully counted in each data run. Since the rotational speed in the vortex-core varies with distance from the center, rotations were counted at the diameter determined previously in plan and profile images. Angular velocity was calculated and from there, circulation and tangential velocity using Equation 4 and Equation 7. Although this velocity measurement method is not perfect, it was more than sufficient for comparing vortices in models of varying size. Results for these parameters are found in the detailed results in Tables A1 – A4 in the Appendix.

Sources of Error

A potential source of experimental error arose in discharge measurements in the various meters used in each experiment. Although time was given for discharge and water surface elevation to stabilize, significant sources of error could have resulted from unsteady inflow, leakage in the flume, and change in surface elevation over time (Padmanabhan and Hecker 1984; Gulliver and Rindels 1987). Since each of the experiments structural requirements necessitated the use of some different materials to construct, there could be error introduced in the lack of exact similitude between them. For example, the prototype used iron to support the force of pressure against the gate, while the smaller experiments used acrylic to support the smaller pressure forces. These

materials have different properties and could have influenced flow patterns. Although care was taken to measure in the same location, measurement of upstream water surface could have introduced error as well.

Since the vortices studied in this research are dynamic moving objects, the subjectivity of data collection from single moments in time is acknowledged. Although this uncertainty was lessened somewhat by taking averages of three data runs for each flow condition, the data is, however, limited by this factor.

Error could also have resulted from the method of measuring dimensions of the vortex core. Since clearly defined, repeatable, structures within the vortex core do not form consistently, human measurement error was introduced with the selection of vortex diameter locations. Error in calculation of length by pixel measurement was also present due to some changes in location of camera lens location and uncertainty in exact location of reference measurements in the photos. The timing of capturing video and simultaneous photos was difficult to get exact. Although multiple measurements were taken of each vortex flow condition, error could have also resulted from the inconsistent and unsteady nature of vortex-flow. To minimize all these errors, multiple readings were recorded and clearly bad results were neglected after analysis. Weighted averages were used to present results.

CHAPTER V

RESULTS

Qualitative Results and Vortex Photographs

The following figures show photographs of vortices in each of the scaled experiments. Figures 18-21 show profiles views of Q1 for the models A, B, C, and D.. Figures 22-25 and Figures 26-29 show profiles views of flow conditions Q2 and Q3, respectively, for each of the models. Each profile photo also contains the locations of D_{V1}, D_{V2}, and D_{V3}, which are shown as red lines overlaid on the image. Refer to Figure 15 for definitions of these locations.

Each of the surface vortices are classified using the six types shown in Figure 6. The formation and change of these stages of vortex formation were examined in these experiments. Dye was used in instances where applicable; however, the vortices did not end up forming a type 3 vortex (which is defined by exhibiting a dye core to the intake). The results of the studies along with vortex types are shown in the following figures.

Figures 30-33 show overhead views of the flow rate Q1 for models A, B, C, and D. Figures 34-37 and Figures 38-41 show overhead views of flow rates Q2 and Q3, respectively, for each of the models.

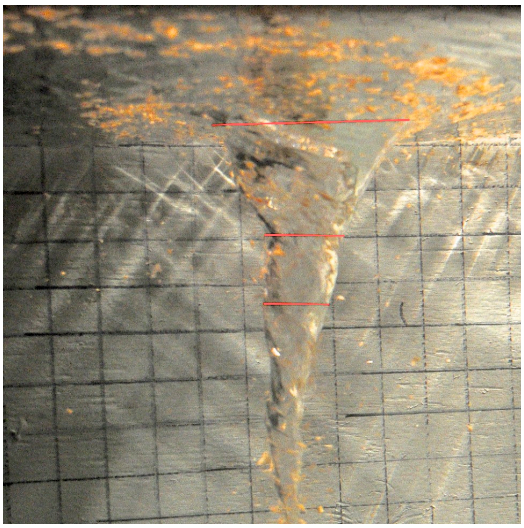

Figure 18. Type 6 vortex at Q1 in model A.

Figure 20. Type 5 vortex at Q1 in model C.

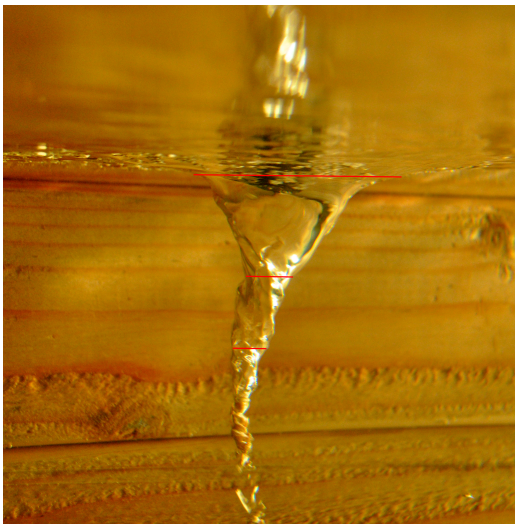

Figure 19. Type 5 vortex at Q1 in model B.

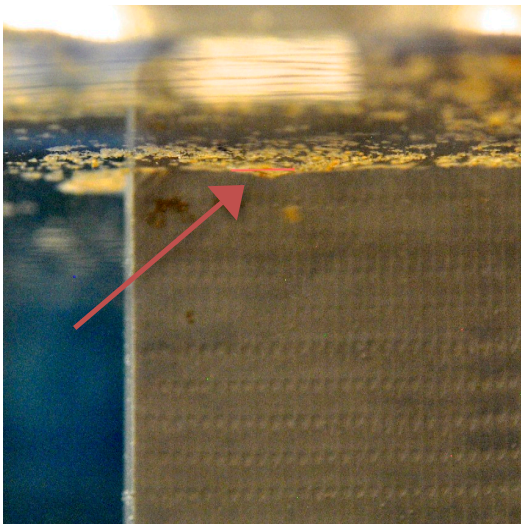

Figure 21. Type 2 vortex at Q1 in model D.

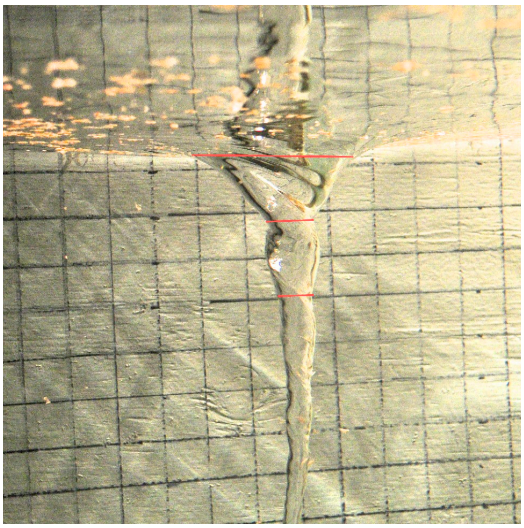

Figure 22. Type 5 vortex at Q2 in model A.

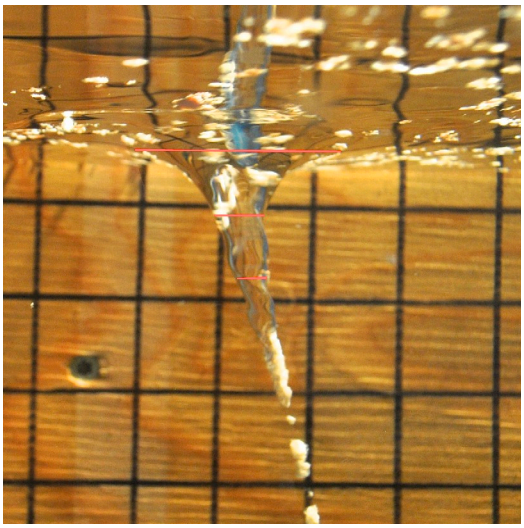

Figure 24. Type 5 vortex at Q2 in model C.

Figure 23. Type 5 vortex at Q2 in model B.

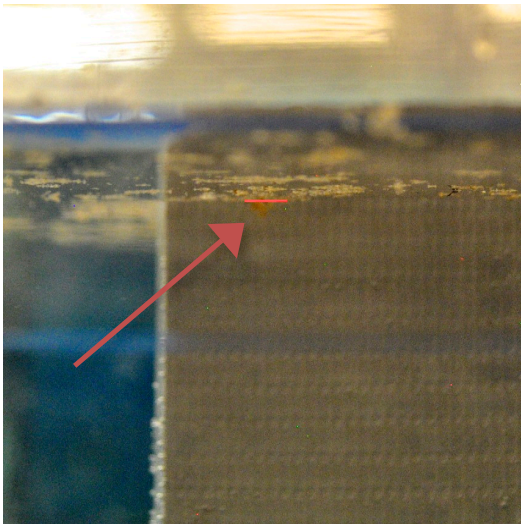

Figure 25. Type 1vortex at Q2 in model D.

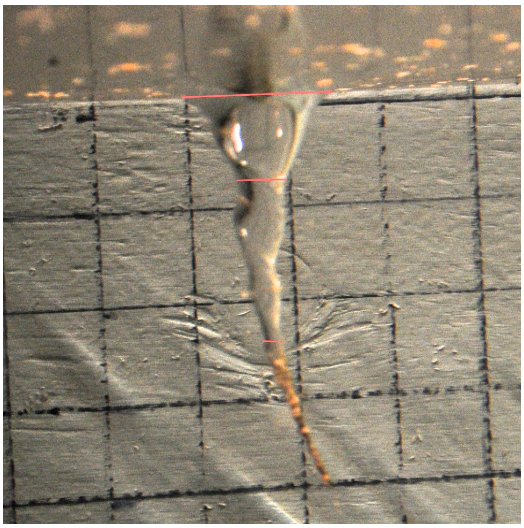

Figure 26. Type 4 vortex at Q3 in model A.

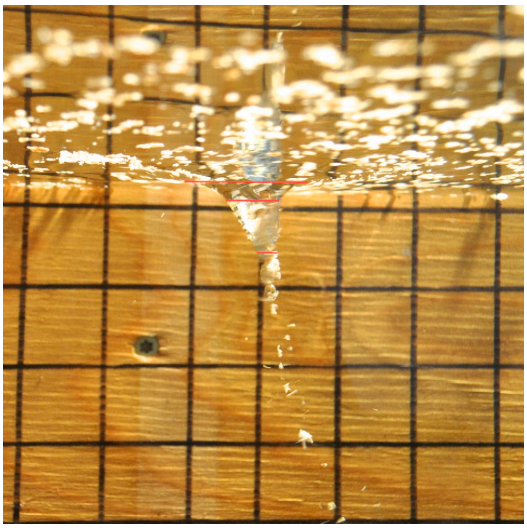

Figure 28. Type 4 vortex at Q3 in model C.

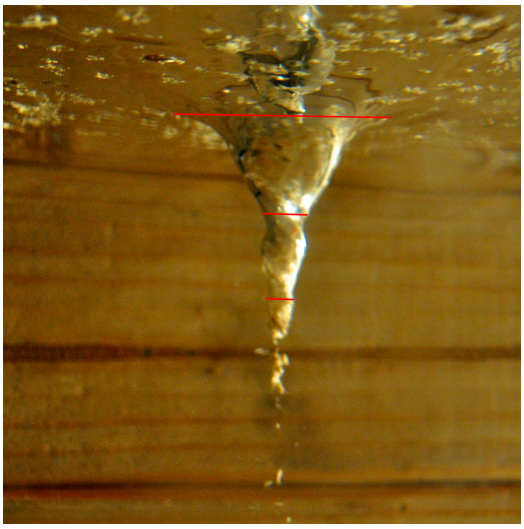

Figure 27. Type 4 vortex at Q3 in model B.

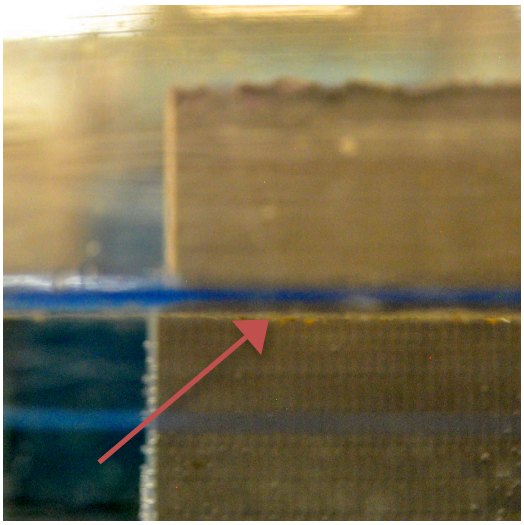

Figure 29. Type 1 vortex at Q3 in model D.

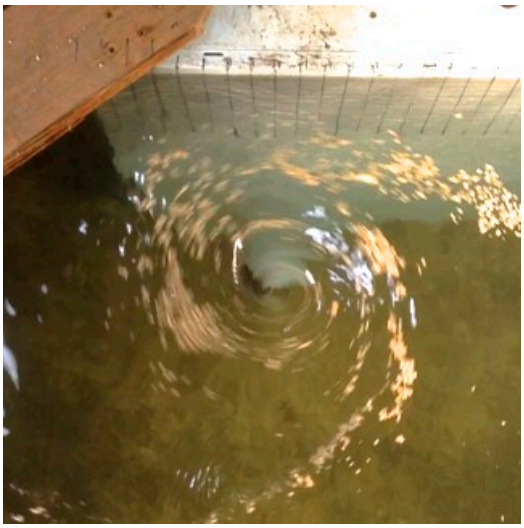

Figure 30. Type 6 vortex at Q1 in model A.

Figure 32. Type 5 vortex at Q1 in model C.

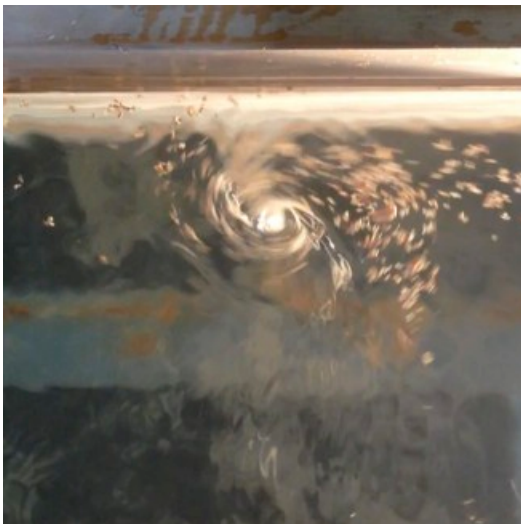

Figure 31. Type 5 vortex at Q1 in model B.

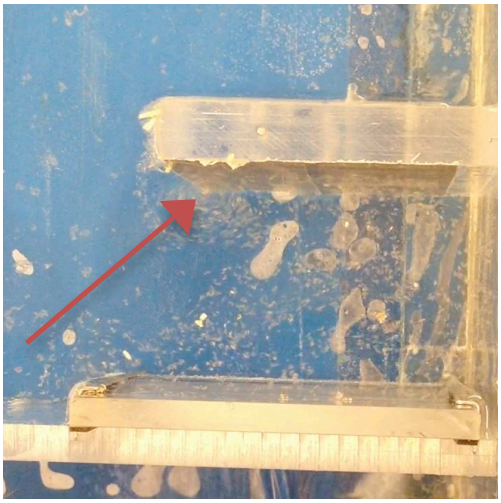

Figure 33. Type 2 vortex at Q1 in model D.

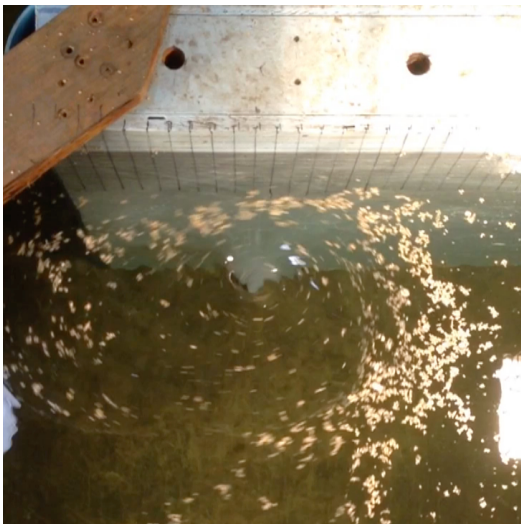

Figure 34. Type 5 vortex at Q2 in model A.

Figure 35. Type 5 vortex at Q2 in model B.

Figure 36. Type 5 vortex at Q2 in model C.

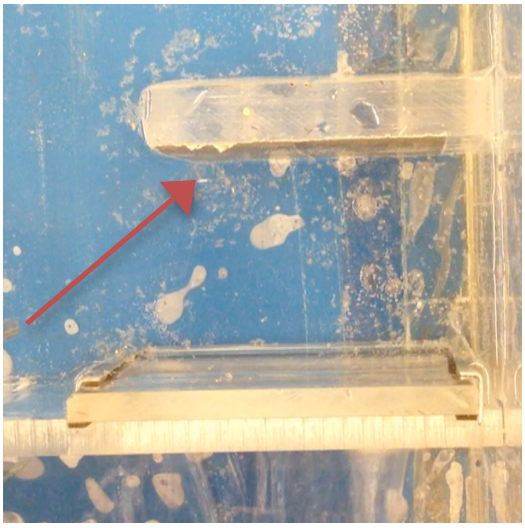

Figure 37. Type 1 vortex at Q2 in model D.

Figure 38. Type 4 vortex at Q3 in model A.

Figure 39. Type 4 vortex at Q3 in model B.

Figure 40. Type 4 vortex at Q3 in model C.

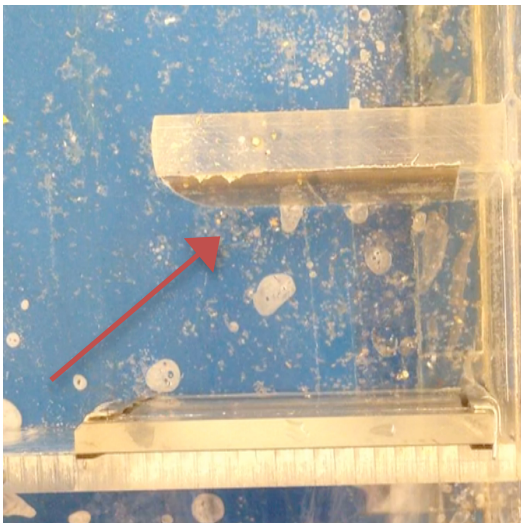

Figure 41. Type 1 vortex at Q3 in model D.

Figures 42-47 show comparisons of vortex profiles across model scales. These figures fall into two categories: scaled and actual measurements. Figures with actual measurements show vortex profile outlines at actual size superimposed on each other, which helps to see how scale affected size. Scaled figures show each vortex superimposed with smaller models scaled up to match the prototype scale. These show effectively that vortex size scaled relatively close to what would be expected in Froude modeling. In each of these figures, a scale is included in inches for reference as well as vortex type for each flow rate.

Quantitative Results

Table 2 contains a summary of the results of the conducted experiments. For each flow condition, three separate runs were taken. The average values from three data runs at each flow condition are reported here. For the diameter DV_1, the average of both profile measurements and top view measurements are reported. Values of D_{V1}, D_{V2}, and D_{V3} in Table 2 are actual measurements, while the scaled diameters are the actual measured diameters in that flow condition scaled back to the prototype.

Results from Table 2 are shown graphically in Figure 48. Here, measured vortex diameter is directly compared with the scaled vortex diameter DV. The scaled diameters were obtained by multiplying measured diameters at that flow condition by their respective length ratio using Equation 9. Figure 49 gives a graph of tangential velocity in each model.

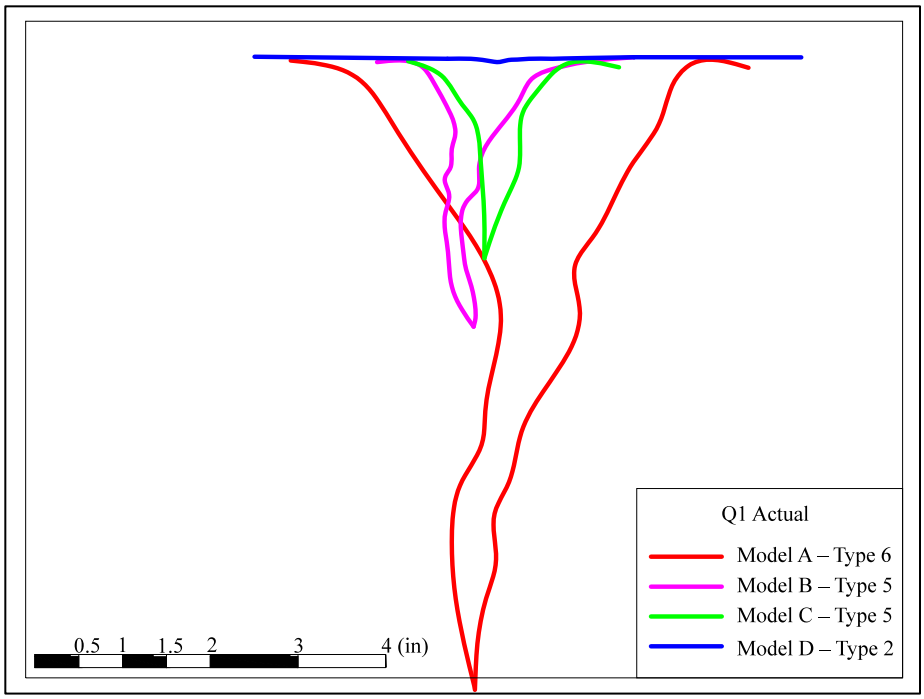

Figure 42. Actual measurement comparison of vortex profiles at Q1.

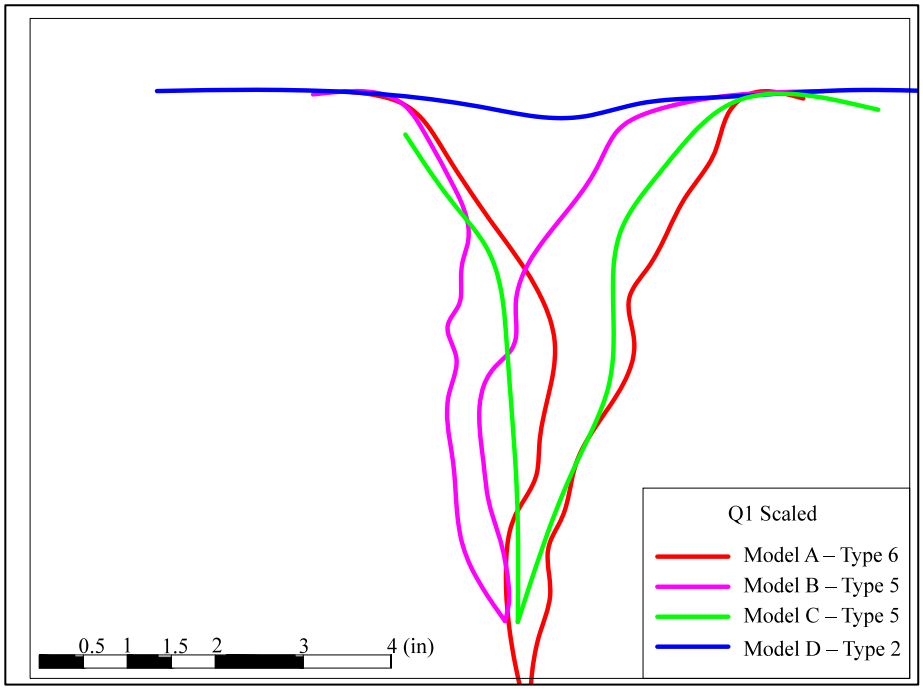

Figure 43. Scaled comparison of vortex profiles at Q1.

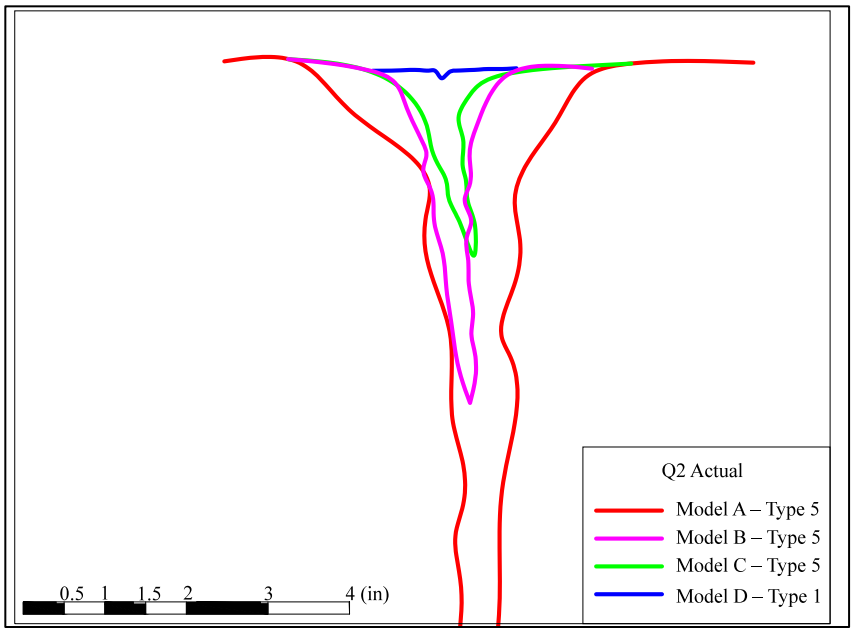

Figure 44. Actual measurement comparison of vortex profiles at Q2.

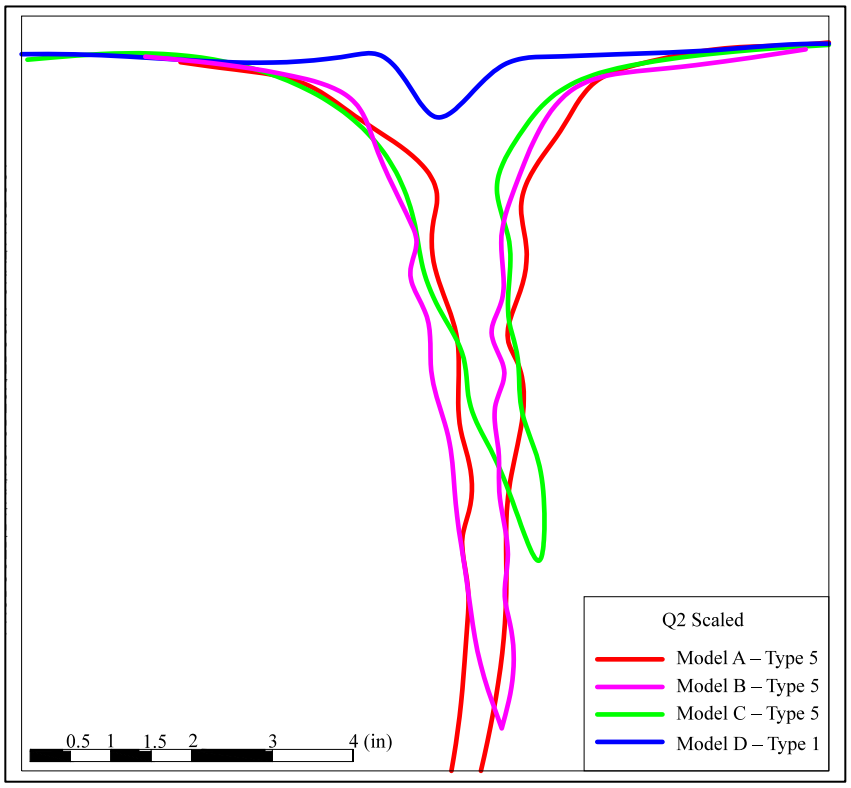

Figure 45. Scaled comparison of vortex profiles at Q2.

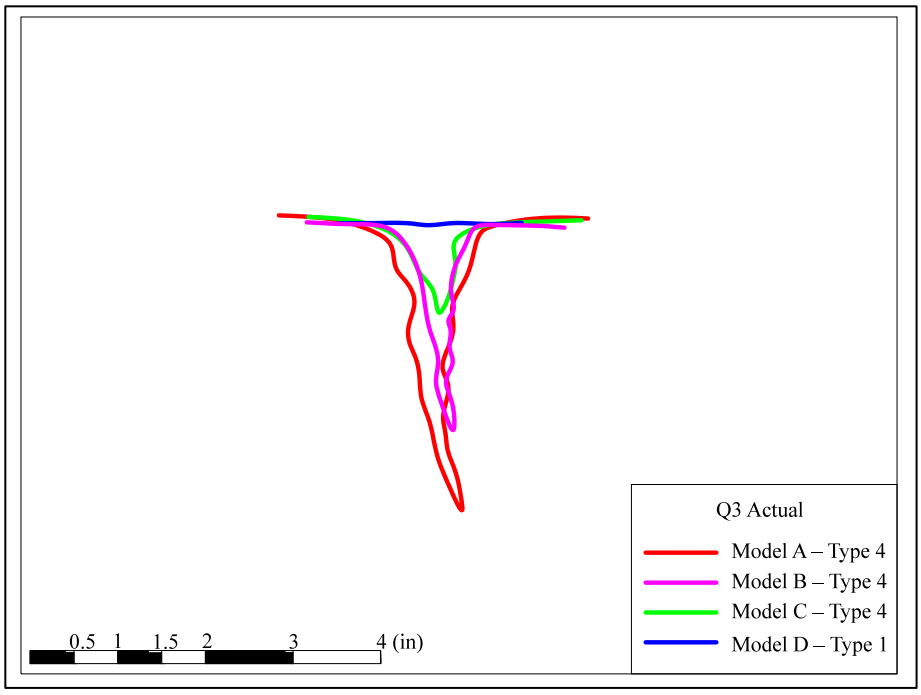

Figure 46. Actual measurement comparison of vortex profiles at Q3

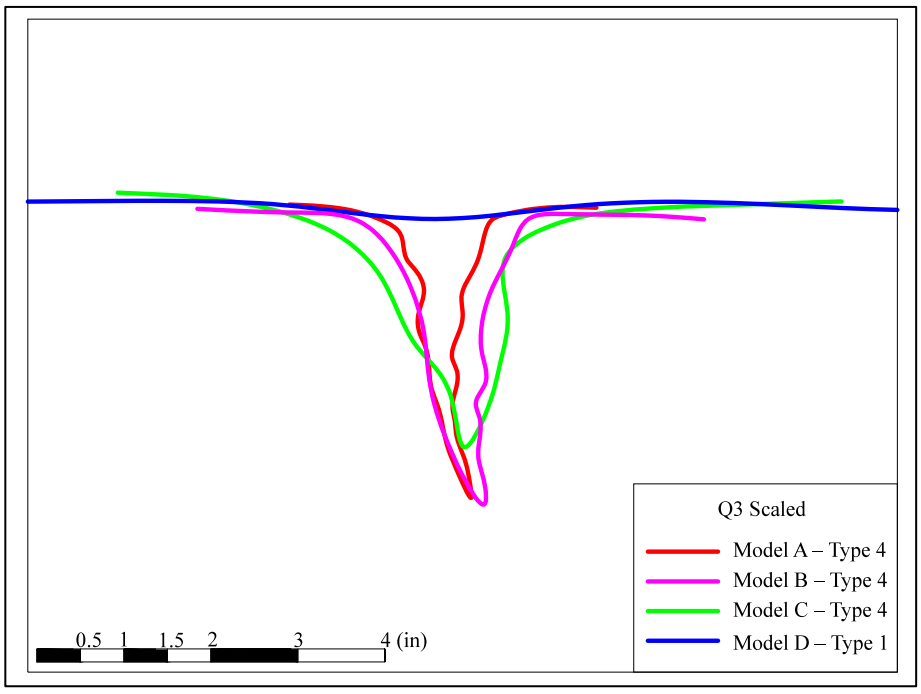

Figure 47. Scaled comparison of vortex profiles at Q3.

Table 2. Summary of experimental results: vortex type and diameter.

Model	Flow Condition	Vortex Type	Vortex Diameter V_1 (in)	Vortex Diameter V_2 (in)	Vortex Diameter V_3 (in)	Scaled Diameter V_1 (in)
A	Q1A	6	3.65	1.08	0.88	3.65
A	Q2A	5	2.94	0.97	0.53	2.94
A	Q3A	4	1.28	0.43	0.08	1.28
B	Q1B	5	1.99	0.51	0.29	3.93
B	Q2B	5	2.11	0.66	0.49	4.17
B	Q3B	4	1.20	0.46	0.28	2.38
C	Q1C	5	1.69	0.44	0.25	4.51
C	Q2C	5	1.68	0.43	0.10	4.63
C	Q3C	4	1.22	0.54	0.16	3.25
D	Q1D	2	0.27	–	–	2.15
D	Q2D	1	0.17	–	–	1.33
D	Q3D	1	0.15	–	–	1.20

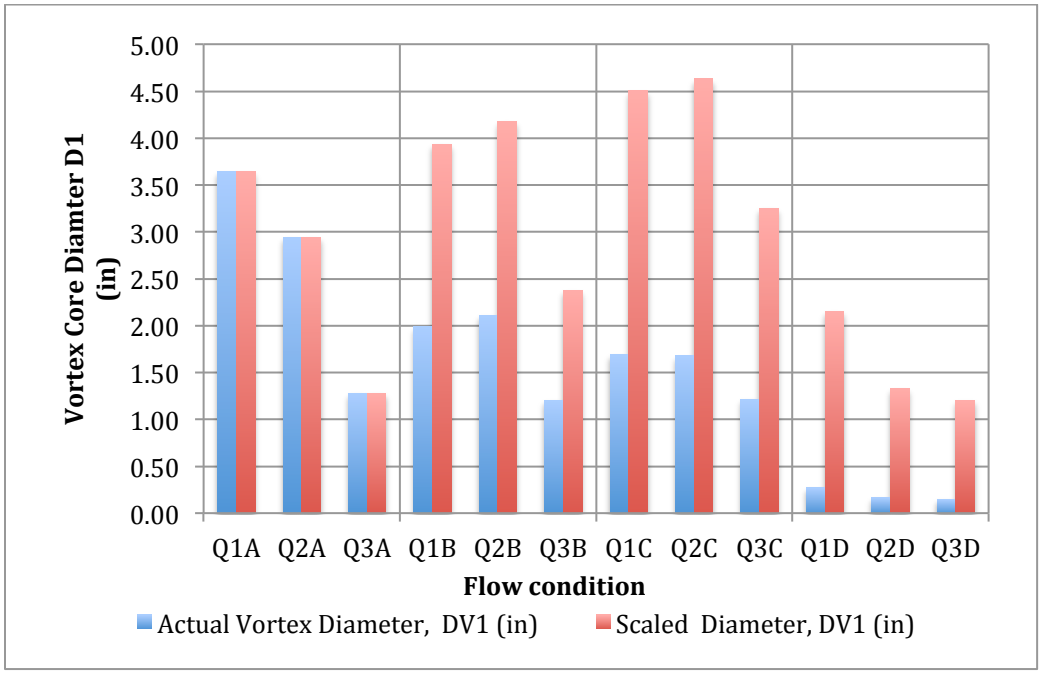

Figure 48. Graph illustrating measured vortex diameter DV_1 versus scaled diameter DV_1 for each experiment.

Figure 49. Tangential velocity in each model flow condition.

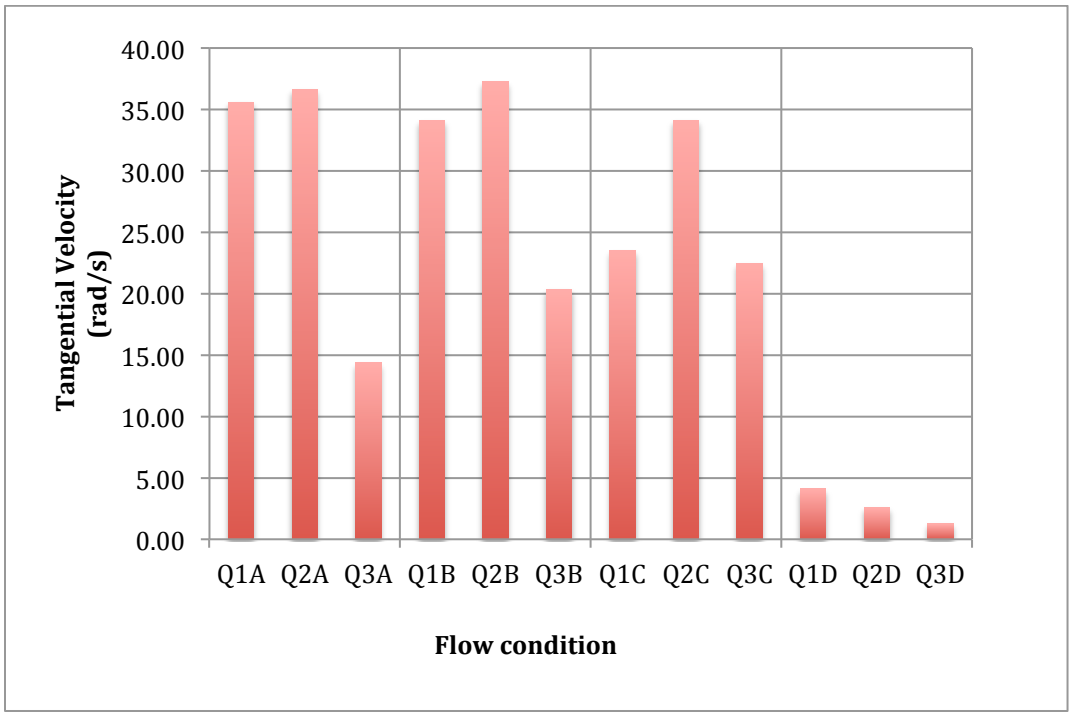

Vortices often did not form in the same area of the experiment across model scales. Table 3 contains results of observed vortex formation location, tangential velocity, and upstream depth. Distances in the X direction are defined as towards the channel wall from the origin, which was defined in Figure 8, while distances in the Y direction are defined as downstream from the origin. These are not scaled values but actual measurements.

The graph in Figure 50 shows visually the scaled locations of vortex formation in each model as shown in Table 3. Distances represented here have been corrected to the prototype sale model scale and points for model scale are represented as a unique symbols. X and Y distances in smaller models have been scaled back to prototype scale for the sake of comparison here. See Figure 8 to reference the location of the obstruction

block shown in Figure 50. Note that negative Y values on the axis label correspond with their respective positive values.

Table 3. Additional results: vortex locations, tangential velocities, and depth measurements.

Model	Flow Condition	Stability (%)	Measured Location, X (in)	Measured Location, Y (in)	Tangential Velocity V_t (rad/s)	Upstream Depth (in)
A	Q1A	0.77	7.50	7.25	35.61	46.8
A	Q2A	0.93	7.27	6.03	36.67	44.4
A	Q3A	0.81	9.35	5.57	14.37	43.2
B	Q1B	0.85	7.43	2.54	34.11	23.3
B	Q2B	0.98	6.33	2.67	37.29	22.2
B	Q3B	1.00	6.15	2.90	20.38	21.5
C	Q1C	0.00	4.37	2.40	23.52	17.7
C	Q2C	0.86	3.73	2.09	34.14	16.7
C	Q3C	0.92	4.09	2.12	22.49	16.4
D	Q1D	1.00	0.73	0.47	4.10	6.0
D	Q2D	1.00	0.55	0.50	2.58	5.6
D	Q3D	1.00	0.85	0.62	1.28	5.4

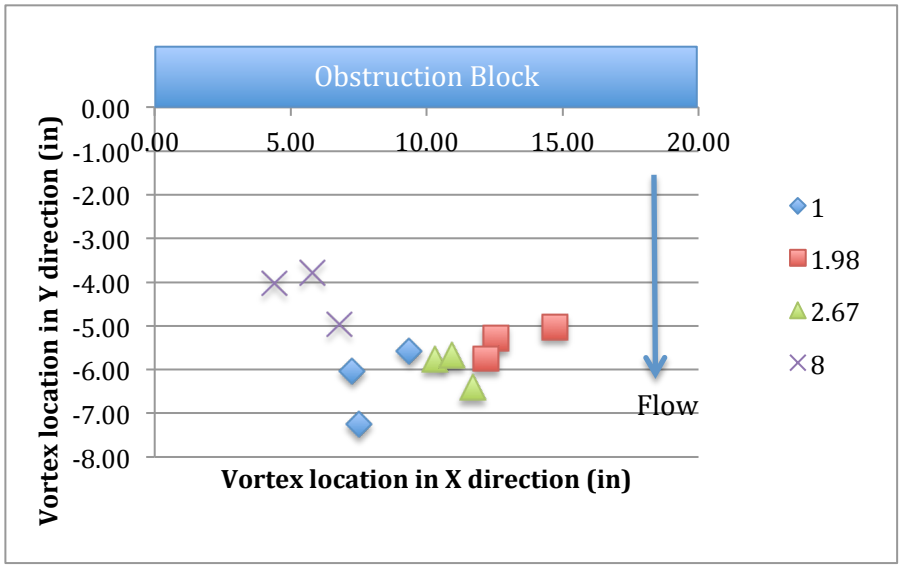

Figure 50. Scaled relative vortex locations.

Table 4. Dimensionless parameters

Model	Flow Condition	Froude Number	Reynolds Number	Weber Number	Elkman Number
A	Q1A	1.33	8.71E+06	3.04E+04	5.70E-08
A	Q2A	1.76	7.22E+06	2.83E+04	5.73E-08
A	Q3A	2.11	1.18E+06	7.16E+03	8.43E-07
B	Q1B	1.35	4.27E+06	2.12E+04	1.21E-07
B	Q2B	1.78	5.74E+06	2.56E+04	1.26E-07
B	Q3B	2.13	1.67E+06	1.01E+04	5.01E-07
C	Q1C	1.33	2.16E+06	1.32E+04	6.92E-07
C	Q2C	1.76	3.42E+06	1.99E+04	1.68E-07
C	Q3C	2.11	1.59E+06	1.13E+04	5.07E-07
D	Q1D	1.33	1.08E+05	9.79E+02	4.26E-05
D	Q2D	1.76	4.58E+04	5.08E+02	1.16E-04
D	Q3D	2.11	1.85E+04	2.26E+02	5.62E-04

CHAPTER VI

DISCUSSION AND CONCLUSION

Discussion

From the experimental results found in Tables 2-4 and Figures 18-50, the following conclusions can be made about scaling effects on vortex flow. The results show changes in vortex strength across the differing model scales. Vortex strength here can be shown qualitatively by its type classification and by inspection through photo or video evidence. Quantitatively, strength is shown by the size of the vortex core and by its tangential velocity.

Results for vortex types are given in Table 2. The experimental results clearly suggest a trend of decreasing vortex strength and type with the increase of model length ratio. This can clearly be seen by vortex type classification across the models for a given flow condition. For instance, at Q1, a type 6 vortex formed in model A, while type 5, type 5, and type 2 vortices formed in models B, C and D, respectively at that flow rate.

As discussed in Chapter III, the Coriolis force here did not play a significant factor in this study because the effects of this force were weak in comparison to the velocity-induced rotation forces in the flow patterns. The velocity-induced vortices were strong enough that Coriolis forces were minor.

Vortex diameter also decreased as model size decreased. Diameter measurements, D_{V1}, D_{V2}, and D_{V3} are found in Table 2 where applicable. In some instances, vortex core measurement was not possible because a developed core did not form at a particular flow condition. In model D at Q3D, no vortex core measurement was taken from the profile

view because a defined core did not form. Similarly, deeper diameter measurements were not taken for any flow condition in model D and D_{V3} measurements were not possible for Q3.

It was observed that as model length ratio increased, Reynolds number decreased, Weber Number decreased, and Elkman Number decreased. Investigation conducted by Anwar et al. (1978) on the onset of air-entraining vortices at a horizontal intakes showed that flow conditions in an air-entraining vortex are not affected by surface tension and viscosity when Reynolds number and Weber number are larger than 3×10^4 and 10^4 respectively.. This also agrees with work conducted by Padmanabhan and Hecker (1984), who concluded that for model Reynolds numbers above $1 \text{ X } 10^5$, the reduced scale models were effective predictors of full-scale intakes. The effects of surface tension and viscosity are affecting the formation of vortices in the scale models. It is not entirely clear from the resultant dimensionless parameters why the vortex size and strength decreased so dramatically in Model D. Since much of the literature had employed experiments that differed from the experiments in this work, it is also difficult to make conclusions from their findings of dimensionless parameters. The calculations of Reynolds number, Weber number, and Elkman number were calculated using tangential vortex velocity and diameter D_{V1}. This method differs from the methods in much of the literature, which also makes comparisons difficult.

However, it is interesting to note that while tangential velocity (Table 2) did not vary greatly for the largest three models, there was a significant decrease in model D. Model D also displayed strikingly weaker vortices, both in size and strength. One of the largest

factors in this observation is the lack of both significant actual approach and actual tangential velocity. The approach velocity, particularly in the region near the arbitrarily defined origin (Figure 8) was a large cause of flow separation and ultimately, swirl leading to vortex formation. The marked decrease in velocity caused a decrease in flow separation around this point, which was a significant factor in the vortex strength reduction.

It should be discussed here that while making observations of model D, a type 6 full air core vortex was formed by modifying the experiment slightly. When a measuring stick was inserted in front of the sluice gate as shown in Figure 51, swirl and tangential velocity increased enough to induce this phenomenon. This agrees with the findings of Anwar et al. (1978) and Jain et al. (1978), suggesting that the leading factor in weak vortex formation in Model D was due to small velocities.

These findings should be taken into consideration for Froude model studies with large length ratios. Although velocities scale as they should according to Equations 9-14, the decreased velocities are insufficient to induce vortex flow to match the vortex conditions (type classification and tangential velocity) seen in larger models.

Figure 48 shows the differences between actual and scaled vortex core diameters. The data shows here that in each model of the prototype, measured diameters were near to their respective scaled diameters. For the model D, measured diameters were larger than their scaled values because defined vortex core boundaries were unclear to determine.

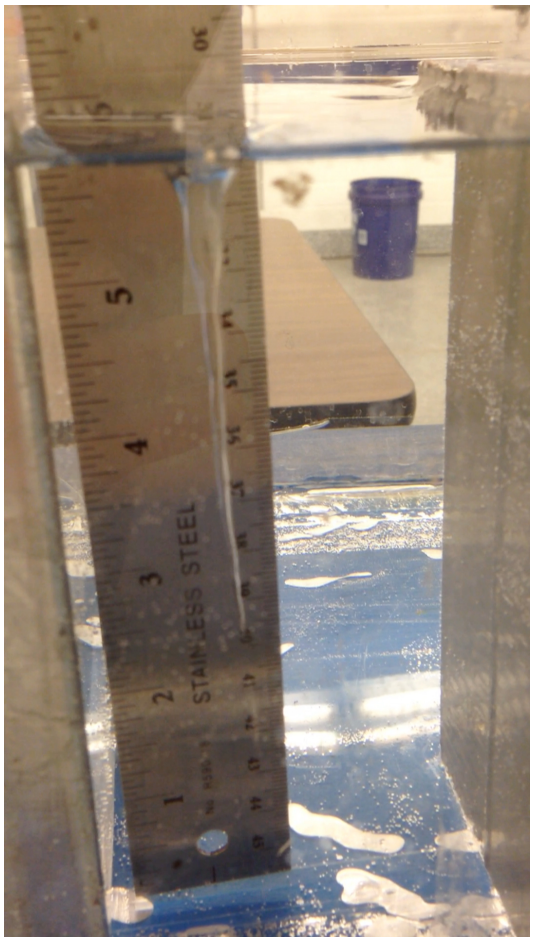

Figure 51. Type 6 full air core vortex forming with a modified approach in model D.

From the vortex outline comparisons shown in Figures 42-47, relative sizes of the vortices observed can be analyzed. The actual measurements show that the vortices indeed decrease in size. The scaled images show that for models B and C, the prototype scaled size of vortices was nearly the same as the prototype vortices. However, the vortices in model D did not scale well in size, strength, and type. This suggests that for relatively small scale ratios (1:2 ~ 1:4), it can be expected that vortex diameter size should scale appropriately. Since vortex strength and type decrease so dramatically in model D, scaling was not as accurate at that size. Further research and observation

should be undertaken for model ratios between 1:2.67 and 1:8 to determine further data points in this area.

These results can be applied to the analysis of physical hydraulic models where vortex formation occurs. For example, in the present work, type 6 fully aerated core vortices formed in model A at Q1 while only type 2 (exhibiting a surface dimple and some swirl) vortices occurred in model D. The results suggest that if vortices form in a scale model, vortex strength will likely increase in the prototype, although size could scale well at small length ratios.

There is an apparent need for further research on this subject. This thesis is not meant to be a comprehensive treatment of the subject; rather, it is an initial examination. Further studies should be carried out using additional technologies such as particle tracking velocimetry (PTV) such as the work done by Kivineimi and Makusa (2009). The PTV system can collect surface flow field data, which can be interpolated to obtain full flow fields. These could then be analyzed according to the Helmholtz vortex theorems and Rankine combined vortex theory principles. Although numerical modeling methods, including computational fluid dynamics (CFD), were not incorporated in this research, they could be used in future work to further this analysis.

Since most of the results were collected by analyzing single moments in time, the depth of analysis could be increased by incorporating observations over time. For example, locations could be plotted over time for given intervals and compared with other model scales. The same methods could be applied to other parameters reported in this work to increase uncertainties and subjectivity.

Additionally, looking at a broader range of model scale ratios can expand upon the present study. The smallest scale ratio studied herein was 1:8 while many model studies are conducted at 1:15 or smaller. It may also be helpful to perform tests with larger channel approach velocities.

Conclusions

This work examined scale effects on vortex formation through the use of a series of identical experiments built at differing scales. Velocity-induced vortices are common occurrences at intakes and can be detrimental to the operation and efficiency of hydraulic structures. Vortices also form in physical hydraulic models often show behavior that differs from the expected hydraulic behavior. Vortices were formed using a sluice gate installed in a level open channel with geometric conditions to create swirl and downward velocity into the sluice gate. Observations were made using simple video and photo evidence from multiple perspectives.

Among the results from this study, a series of photographs were presented detailing the vortices that formed in each experiment. From these photos, comparative outlines of measured and scaled vortices observed in profile were presented. Additionally, quantifiable results including dimensionless parameters were reported and analyzed. It was found that vortex behavior did not scale as expected using Froude scaling principles. As scale length ratios increased and model sized decreased, forces of viscosity, surface tension, and velocity decreased vortex strength. Much of the strength decrease in the smallest model was due to decreased approach and tangential velocity.

Additional research should be undertaken using more extensive methods to collect data and perform analyses at more length ratios in order to come to further conclusions.

REFERENCES

Anwar, H.O. (1965). "Flow in a free vortex." *Water Power* 1965(4), 153-161.

Anwar, H.O. (1967). "Vortices at low head intakes." *Water Power* 1967(11), 455-457.

Anwar, H.O. (1968). "Prevention of vortices at intakes." *Water Power* 1968(10), 393-401.

Anwar, H. O., Weller, J. A., and Amphlett, M. B. (1978). "Similarity of free-vortex at horizontal intake." *J. Hydr.Rsrch.* 16(2), 95-105.

Finnemore, J.E., and Franzini, J. B. (2002). *Fluid mechanics with engineering applications,* 10th edition. McGraw-Hill, New York.

Gordon, J.L. (1970). "Vortices at intakes." *Water Power* 1970(4), 137-138.

Gulliver, J.S., and Rindels, A.J. (1987). "Weak vortices at vertical intakes." *J. Hydr.Engrg.* 113(9), 1101–1066.

Gürbüzdal, F.A. (2009). "Scale effects on the formation of vortices at intake structures." PhD thesis, Middle East Technical University, Ankara, Turkey.

Hecker, G. (1981). "Model-prototype comparison of free surface vortices." *J. Hydr. Div.* 107(10), 1243-1259.

Hite, J., Jr. and Mih, W. (1994). "Velocity of air-core vortices at hydraulic intakes." *J. Hydr.Engrg.* 120(3), 284–297.

Jain, A.K., Kittur, G.R.R., and Ramachandra, J. G. (1978). Air entrainment in radial flow towards intakes. *J. Hydr.Engrg.* 110(11), 1540–1556.

Kiviniemi, O., and Makusa, G. (2009). "A scale model investigation of free surface vortex with particle tracking velocimetry." Masters thesis, Lulea University of Technology, Lulea, Sweden.

Knauss, J. (1987). "Swirling flow problems at intakes." IAHR, Balkema, Rotterdam.

Liggett, James, A. (1994). *Intermediate fluid mechanics*. New ed. edition. McGraw-Hill Education, New York, 69-72.

Odgaard, A. (1986). "Free-surface air core vortex." *J. Hydr.Engrg.* 112(7), 610–620.

Padmanabhan, M., and Hecker, G.E. (1984). "Scale effects in pump sump models." *J. Hydr.Engrg.*, 110(11), 1540-1556.

Schobeiri, Meinhard. (2010). *Fluid mechanics for engineers: A graduate textbook*. Springer, Heidelberg, Germany.

Shapiro, Ascher H. (1962). "Bath-Tub Vortex." *Nature* 196(4859), 1080. doi:10.1038/1961080b0.

Yildirim, N., and Kocabaş, F. (1995). "Critical submergence for intakes in open channel flow." *J. Hydr. Engrg* 121(12), 900–905.

APPENDICES

Testing results are summarized in Tables A1 – A4. Each table includes data collected and observation made regarding each of the test configurations and conditions.

Table A1. Results and computations for Model A.

Vortex Type	Run	Discharge (gpm)	Approach velocity (fps)	Temperature (Deg F)	Gate opening from channel bottom (in)	Upstream head (ft)	Vortex diameter DV1 (in)	Vortex diameter DV2 (in)	Vortex diameter DV3 (in)
6	1	2387.78	0.19	44.1	1.625	3.90	3.78	1.52	1.25
6	2	2387.78	0.19	44.1	1.63	3.90	2.30	0.73	0.46
6	3	2387.78	0.19	44.1	1.63	3.90	4.65	0.98	0.93
5	1	1943.43	0.11	43.4	1.00	3.72	2.28	0.62	0.51
5	2	1943.43	0.11	43.4	1.00	3.72	2.98	1.18	0.26
5	3	1943.43	0.11	43.4	1.00	3.72	3.81	1.12	0.82
4	1	1745.95	0.01	43.7	0.25	3.61	1.55	0.52	0.23
4	2	1745.95	0.01	43.7	0.25	3.61	1.20	0.41	0.00
4	3	1745.95	0.01	43.7	0.25	3.61	1.00	0.36	0.00

Vortex diameter from above (in)	Lateral distance from origin (in)	Vertical distance from origin (in)	Revolutions	Observed time (s)	Angular velocity, ω (rad/s)	Total observation time (s)	Vortex presence observed (s)	Presence (%)	Kinematic Viscosity (ft^2/s)
3.53	6.80	5.46	34.00	10.10	21.15	300.00	230.70	77%	1.56E-05
3.36	7.90	6.76	44.00	13.70	20.18	–	–	–	1.56E-05
4.27	7.80	9.54	23.00	7.70	18.77	–	–	–	1.56E-05
2.24	5	6.11	28	6.5	27.07	300	278	93%	1.58E-05
2.82	6.8	4.92	34	8.6	24.84	–	–	–	1.58E-05
2.94	10	7.06	25	7.1	22.12	–	–	–	1.58E-05
1.50	9.25	4.59	45.00	12.20	23.18	300.00	244.00	81%	1.57E-05
1.43	10.3	6.85	25	6.9	22.77	–	–	–	1.57E-05
1.01	8.5	5.26	26	7.1	23.01	–	–	–	1.57E-05

Table A2. Results and computations for Model B.

Vortex Type	Run	Discharge (gpm)	Approach velocity (fps)	Temperature (Deg F)	Gate opening from channel bottom (in)	Upstream head (in)	Vortex diameter DV1 (in)	Vortex diameter DV2 (in)	Vortex diameter DV3 (in)
5	1	432.84	0.13	42.5	0.82	23.30	1.77	0.65	0.21
5	2	432.84	0.13	42.5	0.82	23.30	2.01	0.34	-
5	3	432.84	0.13	42.5	0.82	23.30	2.21	0.54	0.36
5	1	352.29	0.01	42.1	0.51	22.25	3.19	0.95	0.68
5	2	352.29	0.01	42.1	0.51	22.25	1.85	0.52	0.37
5	3	352.29	0.01	42.1	0.51	22.25	1.75	0.52	0.42
4	1	316.50	0.09	44.4	0.13	21.50	1.11	0.45	0.31
4	2	316.50	0.09	44.4	0.13	21.50	1.43	0.51	0.28
4	3	316.50	0.09	44.4	0.13	21.50	1.25	0.42	0.25

Vortex diameter from above (in)	Lateral distance from origin (in)	Vertical distance from origin (in)	Revolutions	Observed time (s)	Angular velocity, ω (rad/s)	Total observation time (s)	Vortex presence observed (s)	Presence (%)	Kinematic Viscosity (ft^2/s)
1.86	8.03	2.53	51.00	8.40	33.76	117.00	100.00	85%	1.60E-05
1.96	6.65	2.25	56.00	11.00	32.15	–	–	–	1.60E-05
2.11	7.60	2.85	53.00	10.10	36.43	–	–	–	1.60E-05
2.47	6.58	2.2	53	9.7	54.76	120	117	98%	1.61E-05
1.9	4.73	2.73	46	9.4	28.44	–	–	–	1.61E-05
1.49	7.68	3.08	49	9.4	28.66	–	–	–	1.61E-05
1.11	6.44	2.94	53.00	9.80	18.86	103.00	103.00	100%	1.55E-05
1.09	6.21	3.21	48	9.7	22.23	–	–	–	1.55E-05
1.22	5.8	2.55	50	9.8	20.04	–	–	–	1.55E-05

Table A3. Results and computations for Model C.

Vortex Type	Run	Discharge (gpm)	Approach velocity (fps)	Temperature (Deg F)	Gate opening from channel bottom (in)	Upstream head (ft)	Vortex diameter DV1 (in)	Vortex diameter DV2 (in)	Vortex diameter DV3 (in)
5	1	205.62	0.04	35.6	0.61	17.70	1.95	0.48	0.19
5	2	205.62	0.04	35.6	0.61	17.70	1.79	0.37	0.15
5	3	205.62	0.04	35.6	0.61	17.70	0.85	0.48	0.40
5	1	167.36	0.03	37.0	0.38	16.65	1.78	0.38	0.00
5	2	167.36	0.03	37.0	0.38	16.65	1.86	0.48	0.30
5	3	167.36	0.03	37.0	0.38	16.65	1.65	0.43	0.00
4	1	150.35	0.02	34.7	0.09	16.38	1.17	0.41	0.25
4	2	150.35	0.02	34.7	0.09	16.38	1.29	0.55	0.22
4	3	150.35	0.02	34.7	0.09	16.38	1.42	0.66	0.00

Vortex diameter from above (in)	Lateral distance from origin (in)	Vertical distance from origin (in)	Revolutions	Observed time (s)	Angular velocity, ω (rad/s)	Total observation time (s)	Vortex presence observed (s)	Presence (%)	Kinematic Viscosity (ft^2/s)
1.87	5.02	2.48	38.00	8.50	28.09	196.00	182.00	93%	1.81E-05
1.67	3.88	2.59	36.00	7.10	31.86	–	–	–	1.81E-05
2.00	4.22	2.13	39.00	7.10	34.51	–	–	–	1.81E-05
1.62	3.76	2.28	46	7.2	40.14	210	180	86%	1.76E-05
1.67	4.07	2.18	48	8.3	36.34	–	–	–	1.76E-05
1.49	3.36	1.8	40	6.3	39.89	–	–	–	1.76E-05
1.24	4.56	2.00	38.00	6.90	34.60	180.00	165.00	92%	1.84E-05
1.02	4.23	2.33	47	8.5	34.74	–	–	–	1.84E-05
1.16	3.49	2.03	40	7.1	34.96	–	–	–	1.84E-05

Table A4. Results and computations for Model D.

Vortex Type	Run	Discharge (gpm)	Approach velocity (fps)	Temperature (Deg F)	Gate opening from channel bottom (in)	Upstream head (in)	Vortex diameter DV1 (in)	Vortex diameter DV2 (in)	Vortex diameter DV3 (in)
2	1	13.19	0.06	66.0	0.20	6.00	0.23	-	-
2	2	13.19	0.06	66.0	0.20	6.00	0.27	-	-
2	3	13.19	0.06	66.0	0.20	6.00	0.34	-	-
1	1	10.74	0.02	66.0	0.13	5.64	0.18	-	-
1	2	10.74	0.02	66.0	0.13	5.64	0.21	-	-
1	3	10.74	0.02	66.0	0.13	5.64	0.20	-	-
1	1	9.65	0.01	66.0	0.03	5.42	-	-	-
1	2	9.65	0.01	66.0	0.03	5.42	-	-	-
1	3	9.65	0.01	66.0	0.03	5.42	-	-	-

Vortex diameter from above (in)	Lateral distance from origin (in)	Vertical distance from origin (in)	Revolutions	Observed time (s)	Angular velocity, ω (rad/s)	Total observation time (s)	Vortex presence observed (s)	Presence (%)	Kinematic Viscosity (ft^2/s)
0.21	0.97	0.63	57.00	13.00	3.17	180.00	180.00	100%	1.12E-05
0.24	0.65	0.40	37.00	9.10	3.45	–	–	–	1.12E-05
0.32	0.56	0.39	56.00	10.50	5.70	–	–	–	1.12E-05
0.13	0.36	0.52	37	9.5	2.20	180	180	100%	1.12E-05
0.12	0.76	0.66	31	7.3	2.80	–	–	–	1.12E-05
0.16	0.53	0.33	34	7.8	2.74	–	–	–	1.12E-05
0.11	0.83	0.56	21.00	7.90	0.92	180.00	180.00	100%	1.12E-05
0.14	0.85	0.78	18	7.4	1.07	–	–	–	1.12E-05
0.2	0.87	0.52	22	7.5	1.84	–	–	–	1.12E-05